Ontogeny of the Early Triassic Cynodont *Thrinaxodon liorhinus* (Therapsida): Cranial Morphology

SANDRA C. JASINOSKI,[1]* FERNANDO ABDALA,[1] AND VINCENT FERNANDEZ[2]
[1]Evolutionary Studies Institute, University of the Witwatersrand, WITS 2050, Johannesburg, South Africa
[2]European Synchrotron Radiation Facility, 71 rue des Martyrs, Grenoble, France

ABSTRACT

The cranial morphology of 68 *Thrinaxodon liorhinus* specimens, ranging in size from 30 to 96 mm in basal skull length, is investigated using both qualitative and quantitative analyses. From this comprehensive survey, we determined that nine cranial features, including five in the temporal region, separated the sample into four ontogenetic stages. A bivariate analysis of 60 specimens indicated that the skull generally increased in size isometrically, with the exception of four regions. The orbit had negative allometry, a result consistent with other ontogenetic studies of tetrapods, whereas the length of the snout, palate, and temporal region showed positive allometry. The last trend had strong positive allometry indicating that during ontogeny the length of the sagittal crest increased at a much faster rate than the rest of the skull. The large number of changes in the temporal region of the skull of *Thrinaxodon* may indicate a greater development of the posterior fibres of the temporalis musculature from an early ontogenetic stage. For example, the posterior sagittal crest developed much earlier in ontogeny than the anterior crest that formed in adults, and bone was deposited dorsally creating a unified posterior sagittal crest rather than having a suture that spanned the entire depth of the skull roof. In combination with the isometric height of the zygomatic arch and the almost complete absence of the zygomatic arch angulation, these ontogenetic changes suggest that there was greater development of the temporalis relative to the masseter muscles, indicating a strong posterodorsal movement of the mandible in *Thrinaxodon*. Anat Rec, 298:1440–1464, 2015. © 2015 Wiley Periodicals, Inc.

Key words: epicynodont; fossil; skull; growth; allometry; bivariate analysis; sagittal crest

Abbreviations used: BB = basisphenoid-basioccipital; BSL = basal skull length; BW = bicanine width; CT = computed tomography; DSL = dorsal skull length; ESRF = European Synchrotron Radiation Facility; LS = least squares; MA = major axis; MTO = maximum length of the temporal opening (fenestra); MUL = muzzle length; NL = nasal length; OD = orbital diameter; OH = occipital plate height; OL = orbital length; OW = occipital plate width; PAL = palate length; PD = distance between posterior postcanines; POP = postorbital bar to anterior margin of parietal foramen; PSC = posterior margin of the sagittal crest; RMA = reduced major axis; SW = maximum skull width; TEL = temporal region length; UP = upper postcanine tooth row length.

Grant sponsor: DST/NRF Centre of Excellence in Palaeosciences postdoctoral fellowship funding to SJ; Grant sponsor: National Research Foundation (NRF) to FA.

*Correspondence to: Sandra C. Jasinoski, Evolutionary Studies Institute, University of the Witwatersrand, Private Bag 3, WITS 2050, Johannesburg, South Africa. Fax: +27 11-717-6684. E-mail: sandra_jas@hotmail.com

Received 17 August 2014; Revised 12 November 2014; Accepted 14 November 2014.

DOI 10.1002/ar.23116

Published online 23 January 2015 in Wiley Online Library (wileyonlinelibrary.com).

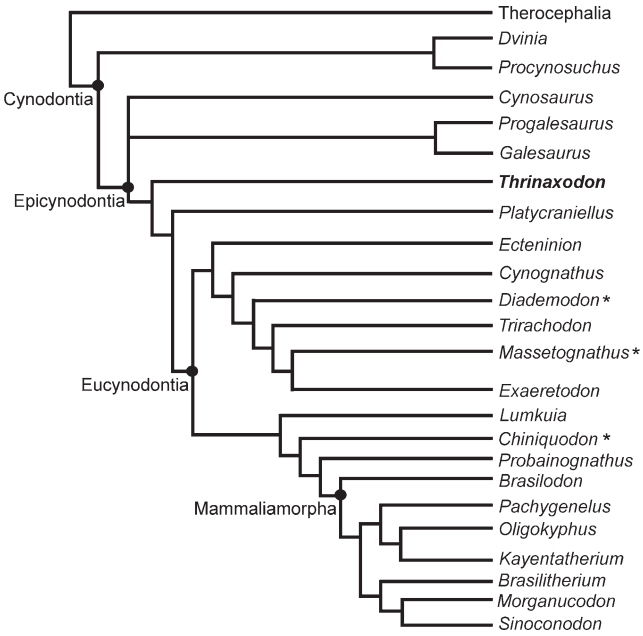

Fig. 1. Phylogenetic tree of the Cynodontia (adapted from Abdala 2007: fig. 9). The phylogenetic position of the eucynodont taxa previously included in allometric studies is indicated with an asterisk (*).

Thrinaxodon liorhinus was a widespread basal cynodont from the Early Triassic of Gondwana, and perhaps the best sampled species of any non-mammaliaform cynodont. There are many well-preserved specimens of *Thrinaxodon*, ranging in size from juvenile to adult, which makes this taxon conducive to studies of ontogenetic change. A survey of the dental morphology and replacement across different ontogenetic stages of *Thrinaxodon* ranging in basal skull length (BSL) of ca. 30–96 mm was recently completed by Abdala et al. (2013). The present study is a continuation of this survey and focuses on the ontogenetic changes in the skull morphology of *Thrinaxodon*.

This taxon was first described by Owen (1887), but assigned the name *Galesaurus planiceps*. Seeley (1894) proposed the new name *Thrinaxodon liorhinus* for this material and for another skull previously referred to as *Nythosaurus larvatus*, based on postcanine morphology. He then assigned the name *Galesaurus planiceps* to previously described material of another basal cynodont contemporary to *Thrinaxodon* but with a shorter biostratigraphical range (see Botha and Smith, 2006; Fig. 1). Since then there have been several studies of cranial variation in *Thrinaxodon*.

Parrington (1936) was the first to compare both the skull and tooth morphology across nine *Thrinaxodon* specimens of different sizes (Table 1). Brink (1955) briefly compared a very small, incomplete *Thrinaxodon* skull with an associated adult skull (Table 1). Estes (1961) described two distorted and slightly incomplete small juvenile specimens and compared their morphology to that of larger specimens (Table 1). The most comprehensive ontogenetic study of this taxon was undertaken by van Heerden (1972), who investigated 22 specimens ranging in size from 35 mm to 92 mm in skull length (Table 1). van Heerden (1972) compared his observations to previous studies by Parrington (1936, 1946), Brink (1955), and Estes (1961), and he also quantified some of these observations. Botha and Chinsamy (2005) investigated histological differences in the postcrania of juvenile and adult specimens of *Thrinaxodon* (Table 1).

The internal structure of the skull of *Thrinaxodon* has also been extensively documented. Fourie (1974) serially sectioned a small adult skull of *Thrinaxodon* and compared his observations to previous cranial studies that used thicker serial sections (Broom, 1938; Olson, 1944). The application of computed tomography (CT) and micro-CT scanning has enabled non-destructive investigations of the internal skull structure of *Thrinaxodon*. *Thrinaxodon* was the first non-mammaliaform cynodont to undergo a CT scan (Rowe et al., 1993) and a recent study used micro-CT to determine tooth replacement patterns in different-sized specimens of *Thrinaxodon* (Abdala et al., 2013).

In most of the previous comparative cranial studies, the number of specimens and the size range between specimens was limited. The smallest, most complete specimens described for *Thrinaxodon* were UCMP 42878 and UCMP 42877 (BSL of 38 mm and 40 mm, respectively; Table 2), and there was a sizeable gap between these early juvenile specimens and the next largest known immature specimen (TM 80A, BSL = 56 mm). Since these studies, several specimens of similar and smaller size relative to the UCMP juveniles have been found (Table 2). The inclusion of these additional early juvenile specimens in the current study and the fact that this taxon has more representatives than any other non-mammaliaform cynodont, can improve our understanding of the morphological changes related to ontogeny. In addition, we investigated six specimens of different sizes using micro-CT, which allowed a comprehensive survey of both external and internal skull morphology across ontogenetic stages.

MATERIALS AND METHODS

Gross Anatomical Observations

A total of 68 *Thrinaxodon liorhinus* skulls from 13 institutions were examined, ranging in BSL from ~30 mm to 96 mm (Table 2; Fig. 2). The majority of these specimens were also part of the tooth replacement study (Abdala et al., 2013). This taxon has been extensively sampled for over 125 years, therefore we expect there will be no extreme outliers missing from our sample and that the largest specimens listed here (Tables 1 and 2) are a good representation of the maximum adult size of *T. liorhinus*. However, there is a gap in the specimens' size representation between BSL of 42 mm (SAM-PK-K10016; -K10017a,b) and 56 mm (TM 80A). In comparison to the more basal and contemporaneous *Galesaurus planiceps*, the sample size of *Thrinaxodon* is much larger, but the adult size of *Galesaurus* is represented by larger specimens (largest BSL of 114 mm; Abdala and Damiani, 2004: table 1).

Most of the specimens observed had been mechanically prepared out of the matrix; however, if the mandible is in situ, the ventral surface of the skull tends not to be fully prepared. A few specimens, especially those from the NHMUK and TM, had been treated with acetic acid, allowing fine detail in the skull to be observed.

TABLE 1. *Thrinaxodon liorhinus* specimens examined in previous ontogenetic studies, listed in increasing size

Parrington (1936)		Brink (1955)		Estes (1961)		van Heerden (1972)		Botha and Chinsamy (2005)	
Specimen	BSL (mm)[a]	Specimen	SL (mm)	Specimen	BSL (mm)[a]	Specimen	DSL (mm)	Specimen	BSL (mm)[a]
UMZC T811 (=R2733)		BP/1/1376 (=BP 274)	-	UCMP 42878	38	UCMP 42877, 42878	35	SAM-PK-K8004	~30
UMZC T812 (=R2739)	61	BP/1/1375 (=BP 273)	82	UCMP 42877	40	TM 1486	35	BP/1/2820	
UMZC T813 (=R2737)	65			UCMP 42865	61	TM 80A	55	SAM-PK-K1395	
UMZC T814 (=R2738)				UCMP 40466	74	NMQR 24[b]	56	SAM-PK-K1121	3 skulls
UMZC T815 (=R2734)	69					RC 107	57	BP/1/5208	73
NHMUK R3731	71					UMZC R2739	61	BP/1/5018	
NHMUK R5480	78					BP/1/472 (=BP M 5)	61	BP/1/4282	82[d]
UMZC T816 (=R2736)	78					NMQR 23[b]	62	BP/1/1730	79[d]
NHMUK R511a	86					UMZC R2737	63		
						TM 80B	63		
						TM 80C[c]	65		
						BP/1/3848	66		
						NHMUK R3731	69		
						BP/1/2776 (=BP 376)	71		
						UMZC T815 (=R2734)	73		
						BP/1/1375 (=BP 273)	78		
						NHMUK R5480	79		
						TM 167	82		
						UMZC T816 (=R2736)	82		
						TM 171	82		
						NMQR 809	84		
						NMQR 810	92		

Abbreviations: BSL, basal skull length; DSL, dorsal skull length; SL, skull length.

[a]BSL measurements taken from the present study (see Table 2) because authors did not provide measurements.

[b]NMQR 23 could not be found in the collections (April 2014). It also appears that van Heerden (1972) switched the specimen number with NMQR 24, which has a DSL of 61 mm (taken by F.A.).

[c]Specimen could not be found in the collections (April 2014) and there is no description of a third skull attributed to TM 80 in the original Transvaal Museum catalogue. van Heerden (1972) did not illustrate or describe TM 80C. He stated that TM 80B was dorsoventrally crushed, so it is likely that his TM 80B is the same specimen as our TM 80B (Table 2).

[d]Botha and Chinsamy (2005) used limb bone measurements to rank specimens in increasing size. They calculated BP/1/4282 as being 97% of adult size and BP/1/1730 as being 100% of adult size.

TABLE 2. List of *Thrinaxodon liorhinus* specimens examined in this study

Specimen	BSL (mm)	Observations
SAM-PK-K8004	~30	Lacks anterior portion of snout
BP/1/1376[ab]	~30	Estimated using complete dentary
TM 1486	~33	Lacks anterior portion of snout
BP/1/5372	37	Micro-CT scanned
UCMP 42878	38	
SAM-PK-K10549	~39	Lacks anterior portion of snout
UCMP 42877	40	
SAM-PK-K10016	42	
SAM-PK-K10017a	42	Specimen with curved body
SAM-PK-K10017b	42	Specimen with straight body
TM 80A	56	Micro-CT scanned
TM 4984[a]	~56	Similar palate length as TM 80A
BP/1/4280	61	
BSP 1934 VIII506	61	
UCMP 42865	61	
FMNH 156	63	
NMQR 24	64	
NMQR 812	64	
UMZC T813	65	
SAM-PK-K1468[a]	~65	Lacks anterior portion of snout
SAM-PK-K10607	66	
RC 107	68	
UMZC T817	~68	Lacks anterior portion of snout
TM 80B	69	
UMZC T815	69	
BP/1/3848	70	
TM 782	~70	Posterior part of skull broken
UCMP 42866	~70	
BP/1/472	71	
BP/1/4263	71	
NHMUK R3731	71	
SAM-PK-K1498	72	
BP/1/5208	73	
BP/1/2776	74	
NMQR 3210[a]	~74	Lacks anterior portion of snout
UCMP 40466	74	
BP/1/7199	75	Micro-CT scanned
TM 180	75	Micro-CT scanned
SAM-PK-K1499	~75	Lacks anterior portion of snout
SAM-PK-K378[a]	~75	Micro-CT; lacks anterior portion of snout
TM K377	76	
SAM-PK-K380[a]	~76	Lacks posterior part of skull
BP/1/2793	77	
BP/1/1693	78	
MCZ 8892[ac]	78	
NHMUK R5480	78	
UMZC T816	78	
BP/1/1730	79	
TM 81a	80	
BP/1/1375[d]	81	
TM 167	81	
BP/1/4282	82	
NHMUK R511	84	
AMMM 4283	85	
BP/1/1737	85	
TM 5074	~85	Posterior part of skull broken
NHMUK R511a	86	
TM 171	~86	
BP/1/5905	87	Micro-CT scanned
NMQR 1416	87	
SAM-PK-K379	89	
TM 166	~89	
BP/1/2824[a]	~90	Lacks posterior part of skull
NMQR 809	91	
NMQR 1864	94	
USNM 22812	94	
NMQR 810	96	
SAM-PK-K1461	96	

Abbreviation: BSL, basal skull length.
[a]Specimen was not included in the bivariate analysis.
[b]Previously designated as BP/1/1375a in Abdala et al. (2013).
[c]The correct BSL is 78 mm and not ~62 mm as listed in Abdala et al. (2013).
[d]Previously designated as BP/1/1375c in Abdala et al. (2013).

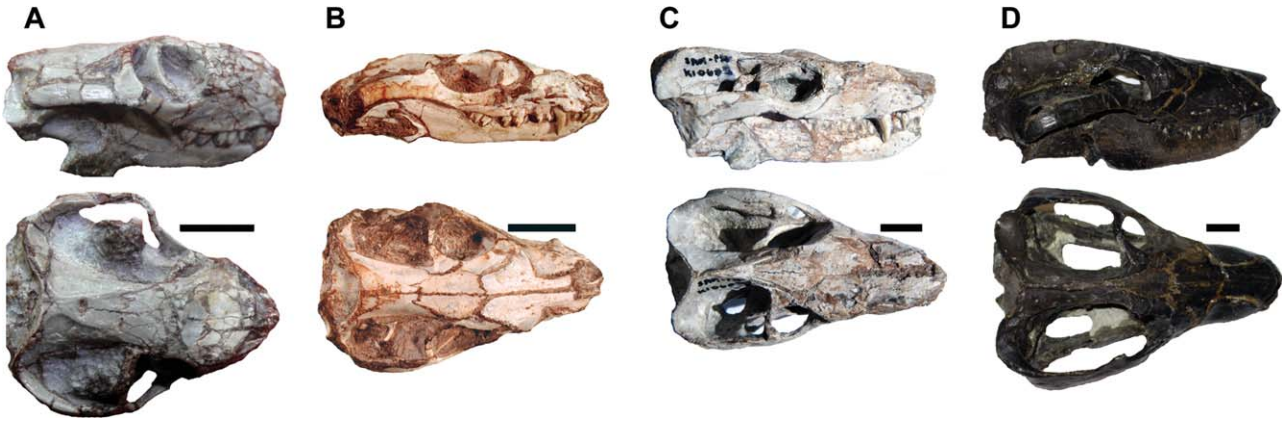

Fig. 2. Specimens of *Thrinaxodon liorhinus* used in this study that show the large variation in size and shape of the skull. (**A**) SAM-PK-K8004, (**B**) SAM-PK-K10016, (**C**) SAM-PK-K10607, (**D**) AMMM 4283. Scale bar equals 10 mm.

Gross observation of the skulls only allowed the surface (ectocranial) trace of the sutures to be examined, a common practice done in many comparative studies (e.g., van Heerden, 1972; Wang et al., 2006); however this may not always indicate the internal structure of the suture (Markey and Marshall, 2007). The internal structure of only a few skulls could be observed, either through serial sections or micro-CT (see below). Because not all specimens have undergone these analyses, some of our observations had to rely on ectocranial trace of the suture, thereby allowing a comparison across the majority of specimens.

Serial Sections

Serial sections of *Thrinaxodon* skulls were undertaken by previous researchers and were used to supplement and confirm our observations from the micro-CT scans. The most comprehensive study was done by Fourie (1974), who serially sectioned specimen NM C354 [dorsal skull length (DSL) of 67 mm] at 0.2 mm intervals. Many of these coronal sections were illustrated and thoroughly labelled in his article. Other studies of serial sections include Broom's (1938) coronal sections of an adult skull of BSL of 88 mm, taken at 4–5 mm intervals. In addition, Olson (1944) made serial coronal sections of a 65 mm skull at 0.37 mm, but he mostly published three-dimensional reconstructions of the skull rather than the individual slices. Parrington (1935: fig. 1A) cut a 64 mm *Thrinaxodon* skull in half near the midline and polished the surface of the sagittal section.

Micro-CT Scanned Specimens

Six skulls of *Thrinaxodon*, ranging in BSL from 37 mm to 87 mm, were micro-CT scanned (Table 2). These specimens are presumed to be immature (BP/1/5372, TM 80A) and mature (SAM-PK-K378, BP/1/7199; TM 180, BP/1/5905) individuals. Specimen TM 80A was scanned using XTH 225 LC (DebTech, DeBeers, Johannesburg, South Africa), with an isotropic voxel size of 50 microns. Specimens SAM-PK-K378 and TM 180 were scanned using XTH 225 ST (X-Sight, Stellenbosch, South Africa). Specimen SAM-PK-K378 was scanned with an isotropic voxel size of 51 microns. Specimen TM 180 has an isotropic voxel size of 50 microns. Three-dimensional reconstructions of the data were undertaken using Mimics (version 13.1, Materialise, Belgium).

Specimens BP/1/5372, BP/1/7199, and BP/1/5905 were micro-CT scanned at the European Synchrotron Radiation Facility (ESRF, Grenoble, France) (see Abdala et al., 2013 for details). Specimens BP/1/5372 and BP/1/7199 (skeleton enclosed in a burrow cast BP/1/5558) was scanned on the beamline ID19 producing data with an isotropic voxel size of 20.24 and 30 microns, respectively. Specimen BP/1/5905 was scanned on the beamline ID17 with a final isotropic voxel size of 45.5 microns. Aviso 6.3 (Visualization Sciences Groups, Merignac, France) and VGStudio MAX 2.2 (Volume Graphics, Heidelberg, Germany) were used for segmentation following similar protocols of previous studies (Abdala et al., 2013).

In addition, the CT-scanned digital atlas of *Thrinaxodon* (UCMP 40466; Table 2) (Rowe et al., 1993), was consulted. This interactive tool allowed observation of labelled digital slices in all three orientations with an interval spacing of 200 microns.

Allometric Analysis

A total of 60 specimens, with a BSL varying from approximately 30 mm to 96 mm, were included in the data set (Table 2). Twenty-three cranial variables were selected for this analysis, and the chosen variables represent shape in different regions of the skull (Fig. 3). The quality of preservation of the studied specimens varied, therefore the sample size (n) of the different measurements ranged between 13 (distance between posterior postcanines, PD) to 58 (muzzle length, MUL) (Table 3). Only two variables, both concerning distance between the upper postcanine tooth rows, have a sample size below 20. Fourteen of the variables were previously used by Abdala and Giannini (2000, 2002), and nine additional variables are presented in the current study (see Table 3; Fig. 3).

All the measurements were recorded to the nearest millimeter, and were taken directly from the specimen using a Mitutoyo digital caliper or from digital photos

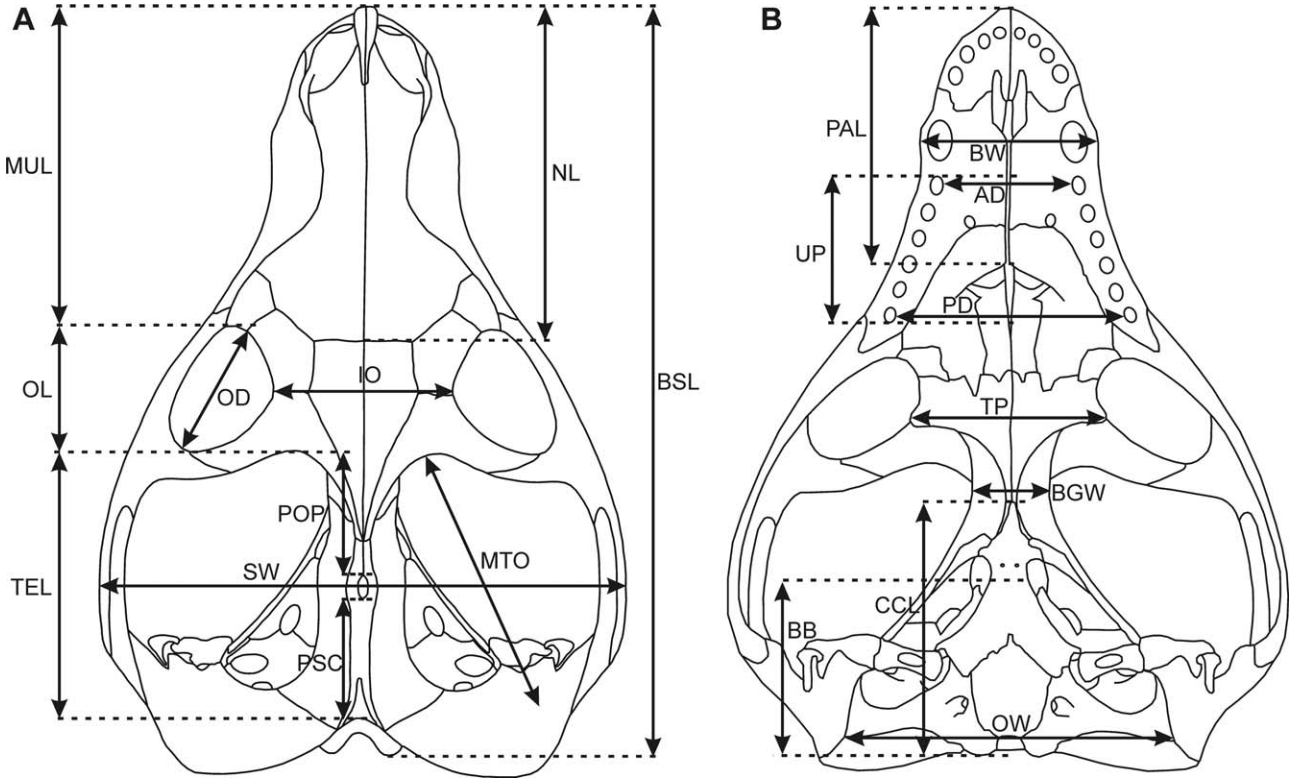

Fig. 3. Schematic illustration of a *Thrinaxodon* skull with measurements and abbreviations used in the bivariate analysis shown in (**A**) dorsal view (modified after Parrington, 1946: fig. 1); (**B**) ventral view (modified after Allin and Hopson, 1992: fig. 28.5E). Abbreviations: BSL, basal skull length. Muzzle: AD, anterior postcanine distance; BW, maxillary bicanine width; MUL, muzzle length; NL, nasal length; PAL, palate length; PD, posterior postcanine distance; TP, transverse process width; UP, upper postcanine tooth row length. Temporal region: MTO, maximum length of the temporal opening (fenestra); POP, postorbital bar to anterior margin of parietal foramen; PSC, posterior margin of parietal foramen to posterior margin of sagittal crest; TEL, temporal region length; SW, maximum skull width; ZH, maximum height of the zygomatic arch (not shown). Orbital region: IO, interorbital distance; OD, orbital diameter; OL, orbital length. Braincase: BB, basisphenoid-basioccipital length; BGW, basicranial girder width; CCL, length from condyle to anterior end of cultriform process; OH, occipital plate height (not shown); OW, occipital plate width.

using the software Digimizer (version 4.2.6.0, MedCalc Software, Ostend, Belgium). All measurements were taken by one individual (F.A.), thus ensuring consistency between measurements. In a couple of cases, measurements taken from the digital photograph were compared to those taken directly from the physical specimen. The resulting measurements were similar, thus indicating high precision between these two methods. When some deformation occurred or a small portion of the skull was lacking (e.g., tip of the snout), a careful approximation of the measurement was made. If the deformation was severe, then the measurement was discarded.

Because several measurements were missing from our data set, it was not possible to use multivariate analysis. Instead, we performed a bivariate analysis which explores the behavior of different log-transformed cranial variables in relation to BSL. The BSL was chosen as the independent variable as it represents a reliable estimator of overall size of the animal (Abdala and Giannini, 2000). For this we employed the equation of allometry (Alexander, 1985), and calculated the slope of the regression line which represents the coefficient of allometry (b). Isometry is indicated by a coefficient equal to one. We employed t-tests to assess significant differences from isometry: negative allometry is indicated by a coefficient significantly less than one, whereas positive allometry is indicated by a coefficient significantly higher than one.

The PAST program (Hammer et al., 2001) was employed for the calculation of the coefficients. Table 3 shows the results obtained using reduced major axis (RMA) method (which assumes error in both dependent and independent variables). However we also inspected the results of the coefficients by employing a least squares (LS) method (assumes error only in the dependent variable) and a major axis (MA) method (minimizes the sum of Euclidean distances from the point to the regression line) (Hammer and Harper, 2006). There were no differences between the allometric trends obtained with RMA and MA as the values of the coefficients were very similar. In Table 3, we only reported coefficients under LS when we obtained different allometric trends in relation to RMA.

Allometric trends using similar bivariate tools were previously studied in the traversodontid *Massetognathus pascuali* (Abdala and Giannini, 2000) and the carnivorous *Chiniquodon theotonicus* (Abdala and Giannini,

TABLE 3. Summary of the regressions on the basal skull length of *Thrinaxodon*

Variable	n	R^2	b_{RMA}	P ($a = 1$)	b_{LS}	P ($a = 1$)	Trend
MUL	58	0.94	1.17	2.40E-05			Pos
NL	42	0.95	0.96	0.2			Iso
PAL	30	0.95	1.15	0.005			Pos
BW	47	0.86	1.1	0.1			Iso
AD	14	0.76	1.11	0.51			Iso
PD	13	0.9	0.81	0.03			Neg
UP	48	0.88	0.93	0.1	0.87	0.009	Iso/Neg
TP	25	0.81	0.96	0.6			Iso
OL	55	0.62	0.65	5.60E-08			Neg
OD	43	0.8	0.87	0.05			Neg
IO	53	0.9	0.99	0.9			Iso
TEL	53	0.93	1.41	1.20E-10			Pos
POP	27	0.8	1.42	0.003			Pos
PSC	26	0.9	1.49	3.50E-05			Pos
MTO	42	0.95	1.29	3.60E-07			Pos
SW	41	0.91	0.95	0.28	0.91	0.05	Iso/Neg
ZH	30	0.83	1.17	0.07			Iso
BB	33	0.8	0.92	0.3	0.82	0.02	Iso/Neg
BGW	29	0.64	1.23	0.1			Iso
OH	34	0.83	1.22	2.00E-02	1.11	0.2	Pos/Iso
OW	44	0.87	0.9	0.06	0.84	0.003	Iso/Neg
CCL	24	0.8	1.08	0.4			Iso

Abbreviations: b_{LS}, coefficient of allometry calculated via least squares; b_{RMA}, coefficient of allometry calculated via reduced major axis method; Iso, isometry; n, sample size; Neg, negative allometry; Pos, positive allometry; R^2, adjusted coefficient of determination. Abbreviations for variables as in Fig. 3.

TABLE 4. Summary of previous cranial allometric studies of non-mammaliaform cynodonts

Taxon	Minimum to maximum number of specimens	Smallest BSL (mm)	Largest BSL (mm)	Reference	Tooth morphology	Diet
Thrinaxodon liorhinus	13–58	30	96	Present contribution	Sectorial toothed	Omnivorous
Diademodon tetragonus	6–11	47	287	Bradu and Grine, 1979	Gomphodont	Herbivorous/ Omnivorous
Massetognathus pascuali	16–31	72	204	Abdala and Giannini, 2000	Gomphodont	Herbivorous/ Omnivorous
Chiniquodon theotonicus	12–18	50	310	Abdala and Giannini, 2002	Sectorial toothed	Carnivorous

Abbreviation: BSL, basal skull length.
The phylogenetic position of these taxa within Cynodontia is indicated on Figure 1.

2002) (Table 4; Fig. 1). In addition, allometric studies were also reported by Grine and collaborators for the African gomphodont *Diademodon tetragonus* (Grine and Hahn, 1978; Grine et al., 1978; Bradu and Grine, 1979). The bivariate technique used in *D. tetragonus* was the Bartlett's best fit (i.e., division of the sample in three groups; Grine et al., 1978). Bradu and Grine (1979) presented the data matrix with measurements of *D. tetragonus* that we used to calculate allometric trends using RMA and thus making them more comparable to the coefficients obtained in *M. pascuali*, *C. theotonicus*, and *T. liorhinus* (Table 5). Liu et al. (2008) performed an ontogenetic study in the Brazilian traversodontid *Massetognathus ochagaviae*, but the specimens are frequently deformed (Liu et al., 2008) with the bones swollen and in some cases exploded by the effect of calcite and hematite cementation (Holz and Schultz, 1998); therefore we decided not to include this taxon in our comparison.

Institutional Abbreviations

Cranial material of *Thrinaxodon* was examined from the following institutions: AMMM, McGregor Museum, Kimberley, South Africa; BP, Evolutionary Studies Institute (formerly Bernard Price Institute for Palaeontological Research), University of the Witwatersrand, Johannesburg, South Africa; BSP, Bayerische Staatssammlung für Paläontologie und Historische Geologie, Munich, Germany; FMNH, Field Museum of Natural History, Chicago, IL; MCZ, Museum of Comparative Zoology, Harvard University, Cambridge; NHMUK, The Natural History Museum, London, UK.; NM or NMQR, National Museum, Bloemfontein, South Africa; RC, Rubidge Collection, Wellwood, Graaff Reinet, South Africa; SAM, Iziko South African Museum, Cape Town, South Africa; TM, Ditsong National Museum of Natural History, Pretoria (formerly Transvaal Museum), South Africa; UCMP, Museum of Paleontology, University of California, Berkeley; UMZC,

TABLE 5. Allometric trends of *Thrinaxodon* compared with three eucynodont taxa

Variable	*Thrinaxodon liorhinus*	*Diademodon tetragonus*	*Massetognathus pascuali*	*Chiniquodon theotonicus*
MUL	Pos (1.17)	Iso (1.01)	Neg (0.94)	Iso (1.02)
PAL	Pos (1.15)	Iso (0.98)	Neg (0.83)	Pos (1.08)
BW	Iso (1.1)	Iso (1.02)	Iso (0.99)	Pos (1.24)
AD	Iso (1.11)		Iso (1.07)	Iso (1.04)
PD	Neg (0.81)		Neg (0.82)	Iso (0.99)
UP	Iso (0.93)	Neg (0.93)	Neg (0.83)	Iso (0.93)
TP	Iso (0.96)	Iso (0.96)	Neg (0.61)	
OL	Neg (0.65)		Neg (0.91)	Iso (0.97)
OD	Neg (0.87)	Neg (0.69)	Neg (0.73)	
IO	Iso (0.99)	Iso (0.92)	Iso (1.09)	Iso (1.09)
TEL	Pos (1.41)		Pos (1.25)	Pos (1.12)
MTO	Pos (1.29)	Iso (1.10)		
SW	Iso (0.95)	Pos (1.17)[a]	Pos (1.30)	Pos (1.12)
ZH	Iso (1.17)	Pos (1.21)	Pos (1.37)[b]	Pos (1.24)
BB	Iso (0.92)		Neg (0.87)	Pos (1.28)
OH	Pos (1.22)		Iso (1.01)	Iso (0.94)
OW	Iso (0.9)	Pos (1.28)	Iso (1.12)	Iso (1.11)

Allometric data (via reduced major axis) for *Massetognathus pascuali* taken from Abdala and Giannini (2000); *Chiniquodon theotonicus* from Abdala and Giannini (2002). We calculated allometric trends using reduced major axis for *Diademodon tetragonus* using data from Bradu and Grine (1979).
[a]Marginally significant (p=0.07)
[b]Result from the re-analysis of data of Abdala and Giannini (2000).
Abbreviations: Iso, isometry; Neg, negative allometry; Pos, positive allometry.
Abbreviations for variables as in Figure 3.

University Museum of Zoology, Cambridge, UK.; USNM, United States National Museum, Smithsonian Institution, Washington.

RESULTS

Allometric Analysis

Table 3 and Figure 4 show results from the bivariate analyses of allometry of *Thrinaxodon*. All the variables were explained by the linear allometrical model with the R^2 coefficient varying from 0.62 for the orbital length (OL) to 0.95 for the nasal length (NL), palate length (PAL), and maximum length of the temporal opening (MTO) (19 variables show R^2 equal or higher than 0.8). Residues do not show outliers and there are no systematic trends across the sample.

Variation of RMA allometric coefficient (b) ranges from 0.65 for OL to 1.49 for the length from posterior margin of

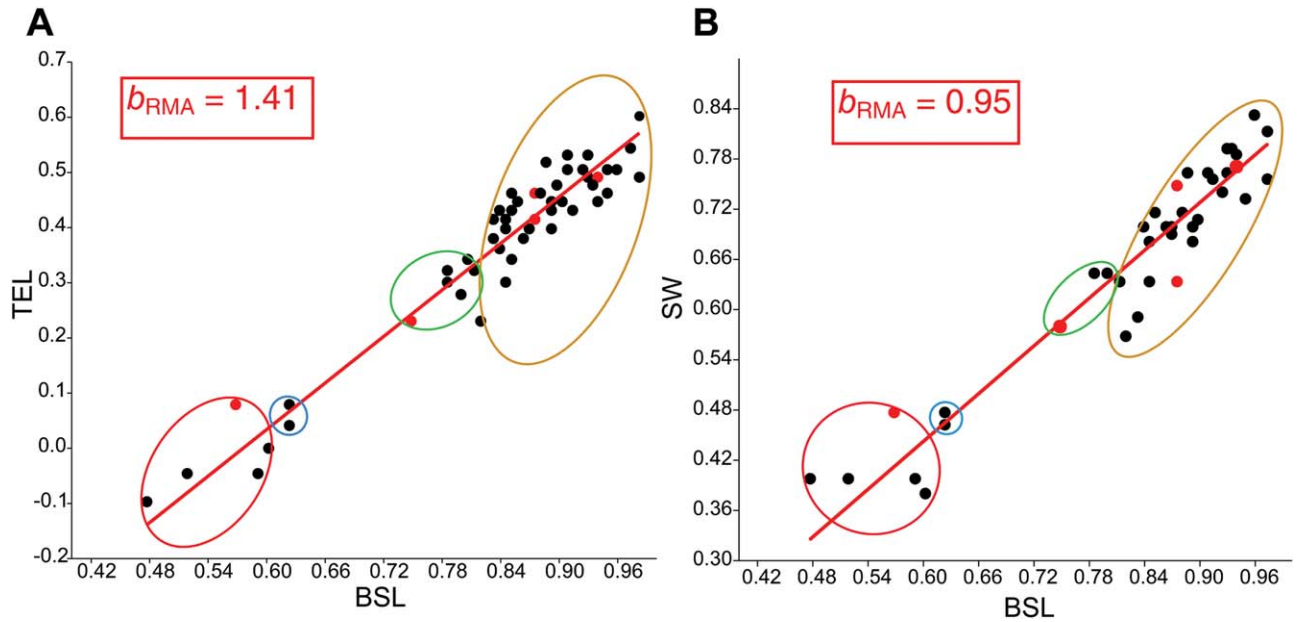

Fig. 4. Bivariate graphs (log-transformed) of *Thrinaxodon*. (**A**) TEL versus BSL showing strong positive allometry, (**B**) SW versus BSL showing isometry with RMA. On both graphs, the inset is the coefficient of allometry, the red dots indicate specimens that were micro-CT scanned (Table 2), and the coloured ovals demarcate the four ontogenetic classes of *Thrinaxodon* (red: early juveniles; blue: late juveniles; green: subadults; brown: adults). Abbreviation: b_{RMA}, coefficient of allometry calculated via reduced major axis method.

TABLE 6. List of cranial features of *Thrinaxodon liorhinus* that changed during ontogeny

Character	BSL (mm)	Ontogenetic stage	Position in skull
Nasal-Frontal suture morphology: inverted V-shaped	≤42[a]	Juvenile	Snout
Nasal-Frontal suture morphology: transverse, inverted V-shaped, or intermediate morphology	56–66	Subadult	
Nasal-Frontal suture morphology: transverse	≥69[b]	Adult	
Presence of paired interpterygoid vacuities	≤40[c]	Juvenile	Posterior palate
Absence of paired interpterygoid vacuities	≥56	Subadult, Adult	
Frontal-Parietal suture morphology: M-shaped interdigitated	≤37	Early Juvenile	Temporal
Frontal-Parietal suture morphology: transverse	~39–42	Late Juvenile	
Frontal-Parietal suture morphology: M-shaped interdigitated	≥56	Subadult, Adult	
Posterior projection of postorbital: ventral and incipient dorsal processes	≤42	Juvenile	Temporal
Posterior projection of postorbital: well-developed ventral and dorsal processes forming a 'C'	≥56	Subadult, Adult	
Sagittal crest not developed	≤40	Early Juvenile	Temporal
Development of posterior sagittal crest	≥42[d]	Late Juvenile	
Development of anterior sagittal crest	≥69	Adult	
Parietal foramen shape: ovoid (transversely wide) to circular	≤40	Early Juvenile	Temporal
Parietal foramen shape: ellipsoid (transversely narrow and anteroposteriorly long)	≥42	Late Juvenile-Adult	
Posterior parietal-parietal suture extends close to the dorsal edge of the parietal bones	37	Juvenile	Temporal
Posterior parietal-parietal suture is present in the ventral half of the parietal bones	56	Subadult	
Posterior parietal-parietal suture is present only near the ventral edge of the parietal bones	75	Adult	
Supraoccipital is bulbous and projects further posterior than the occipital condyle	≤56	Immature	Occiput
Occipital condyle protrudes further posteriorly than the supraoccipital	≥61	Mature	
Absence of an external occipital crest	<61	Immature	Occiput
Presence of an external occipital crest	≥61[e]	Mature	
Upper postcanines: bicuspid and tricuspid teeth are present	≤42[f]	Juvenile	Dental
Upper postcanines: bicuspids are rare (usually PC1/2), tricuspids lack cingular cusps	56–68[f]	Subadult	
Upper postcanines: bicuspids are rare (usually PC1/2), tricuspids may have cingular cusps	≥69[fg]	Adult	
Rate of incisor replacement is slower (e.g., replacement in first and third positions)	≤56[f]	Immature	Dental
Rate of incisor replacement is faster (replacement in nearly all incisors)	≥75[f]	Mature	
Rate of canine replacement is faster (e.g., two canines occasionally occur at the same time)	≤42[f]	Immature	Dental
Rate of canine replacement is slower	>42[f]	Mature	

From these qualitative characters, the sample of *Thrinaxodon* can be divided into four ontogenetic stages: early juvenile, late juvenile, subadult, and adult.
Abbreviations: BSL, basal skull length; PC, postcanine.
[a]Specimen SAM-PK-K10016 is an exception.
[b]Four adult specimens have a definite inverted V-shaped nasal-frontal suture.
[c]Palatal region is not prepared in specimens of BSL 42 mm (Table 2).
[d]Specimen SAM-PK-K10017b is an exception.
[e]Five specimens do not have an external occipital crest.
[f]Observation made by Abdala et al. (2013).
[g]Not all adult specimens have cingular cusps.

the parietal foramen to the posterior margin of the sagittal crest (PSC) (Table 3). In nine variables there was a rejection of isometry obtained by the three methods: negative allometry for OL, orbital diameter (OD), and PD; positive allometry for MUL, PAL, length from the postorbital bar to the anterior margin of the parietal foramen (POP), PSC, temporal region length (TEL), and MTO. Five variables were considered allometric by only one of the methods: negative allometry by LS in upper postcanine tooth row length (UP), maximum skull width (SW), occipital plate width (OW), and basisphenoid-basioccipital length (BB); and positive allometry with RMA in occipital plate height (OH).

Qualitative Differences During Ontogeny

The following are the results of a qualitative survey highlighting cranial differences observed in specimens of different sizes. To that effect we divided our observations in juveniles and adults according to skull size (Table 6), and highlighted character associations that may improve our recognition of different ontogenetic stages in the sample.

Snout and Palate

Nasal-frontal suture on surface. The ectocranial trace of the nasal-frontal suture on the surface of the snout was a feature proposed by Estes (1961) to separate juvenile from adult specimens. Estes (1961) stated that in juveniles the frontals have anterior-projecting spines forming an arrow-shaped (inverted V-shaped) nasal-frontal suture, whereas the nasal-frontal suture is transverse in adult specimens. In the dorsal view of the juvenile specimen, the nasal-frontal suture and the prefrontal-frontal sutures nearly form a straight line relative to each other (Estes, 1961).

In this study, all specimens with a BSL of 42 mm or less, with the exception of SAM-PK-K10016, have an anterior frontal projection that forms an inverted V-shaped ectocranial suture trace (Table 6; Fig. 5A). Note that we interpreted specimen BP/1/1376 as having an inverted V-shaped suture and not a transverse suture as illustrated by Brink (1955: fig. 26a), and SAM-PK-K10016 has an intermediate morphology between an inverted V-shaped and a transverse suture. In specimens with a BSL of 56–66 mm (Table 2), there is a transitional shift wherein six specimens have a transverse suture with some anteroposterior-oriented interdigitations, while four specimens have an inverted V-shaped suture or an intermediate morphology (Fig. 5B). In larger individuals (BSL $\geq$ 69 mm), the majority of specimens have a transverse suture with some variation in the number and size of the anteroposterior aligned interdigitations (Fig. 5C). However, four adult specimens with BSL of 71–94 mm have a definite inverted V-shaped nasal-frontal suture (NHMUK R3731, SAM-PK-K380, TM 5074, USNM 22812; Fig. 5D). Therefore, there is some variation in the morphology of the nasal-frontal suture, but for the most part, the inverted V-shaped suture morphology occurs in immature specimens.

Nasal-nasal suture on surface. There is some intraspecific variation in the nasal-nasal suture, but it is difficult to detect an ontogenetic pattern. In several specimens, the suture is fairly straight for most of its length, but interdigitations occur near the midlength of the snout, close to the "apex" of the scarf maxilla-nasal suture (Fig. 6). Even in one of the smallest specimens (BP/1/5372), there is at least one interdigitation in this region.

Secondary palate. In our survey, the majority of specimens do not have an exposed or fully preserved secondary palate. In those that do, we took into account the preservation and the preparation (acid, mechanical, and/or digital preparation) of the specimens. For example, specimens that are distorted may have palatal shelves that slightly overlap at the midline (Fig. 7A), and therefore were not considered here.

The mammalian bony secondary palate is formed by the closure of the premaxillae, maxillae and palatine bones along the midline of the palate (Thomason and Russell, 1986). In *Thrinaxodon*, the anterior part of the secondary palate, formed by the premaxillae and maxillae, is perforated by a long foramen incisivum and the anterior end of the vomer is clearly visible at the midline (Fig. 7). In most *Thrinaxodon* specimens we observed that the palatal shelves (intermaxillary and interpalatine) do not contact each other at the sagittal midline of the secondary palate. The maxillae do not come into contact at the midline in any undistorted specimen, and the vomer septum is visible within the intermaxillary cleft (Fig. 7); however, the gap between the palatines tends to be smaller (the vomer septum is sometimes visible in the cleft), and in a few cases the palatines almost contact each other at the midline. In summary, the bony palatal shelves of *Thrinaxodon* are not tightly articulated along the midline. The lack of closure of the secondary palate does not appear to be an ontogenetic feature because it was observed in both immature and adult specimens (Fig. 7).

The medial edges of the interpalatine and intermaxillary sutures of *Thrinaxodon*, visible in micro-CT (e.g., BP/1/5372) and under the microscope (e.g., TM 81a), are relatively flat with some bony rugosities [sutura harmonia of Fourie (1974)] (Fig. 7D). The secondary palate of *Thrinaxodon* differs from that of mammals, in which the paired bones are in close contact at the midline (e.g., Rafferty et al., 2003: fig. 6; Thomason and Russell, 1986: fig. 3) and have a comparatively longer posterior extension.

Interpterygoid vacuity. In the region between the palatal region and the basicranial girder is a structure designated as the interpterygoid vacuity. We interpret the vacuity as an opening through the basicranial girder, medially bounded by the rostrum (cultriform process) of the parasphenoid and laterally by the pterygoids (see also Martinelli, 2009). This delimitation implies that the structure consists of paired openings on either side of the rostrum.

The presence of paired interpterygoid vacuities was associated with the juvenile condition in *Thrinaxodon* (e.g., Estes, 1961; Hopson and Barghusen, 1986), and is clearly supported by our extensive survey. At least one of the paired interpterygoid vacuities is visible in the small specimens UCMP 42877, UCMP 42878, TM 1486, and BP/1/5372 (Fig. 8A). In UCMP 42878, there are two vacuities clearly visible between the parasphenoid rostrum and the medial margin of the pterygoids, whereas only one of the paired vacuities is visible in UCMP 42877 due to distortion of the skull. In TM 1486 and BP/1/5372 (Fig. 8A), the cultriform process of the parasphenoid, which normally divides the vacuity, is missing or deformed. The interpterygoid vacuities are absent in all specimens with a BSL of 56 mm or greater; however it is not known if they are present in the specimens with a BSL of 42 mm (Table 2) due to lack of preparation of the palate. In the intermediate-sized skull of TM 80A, there are deposits of bone lateral to the cultriform process indicating that the interpterygoid vacuities were infilled (Fig. 8B). In larger specimens, this area becomes constricted because the paired pterygoids compress against the

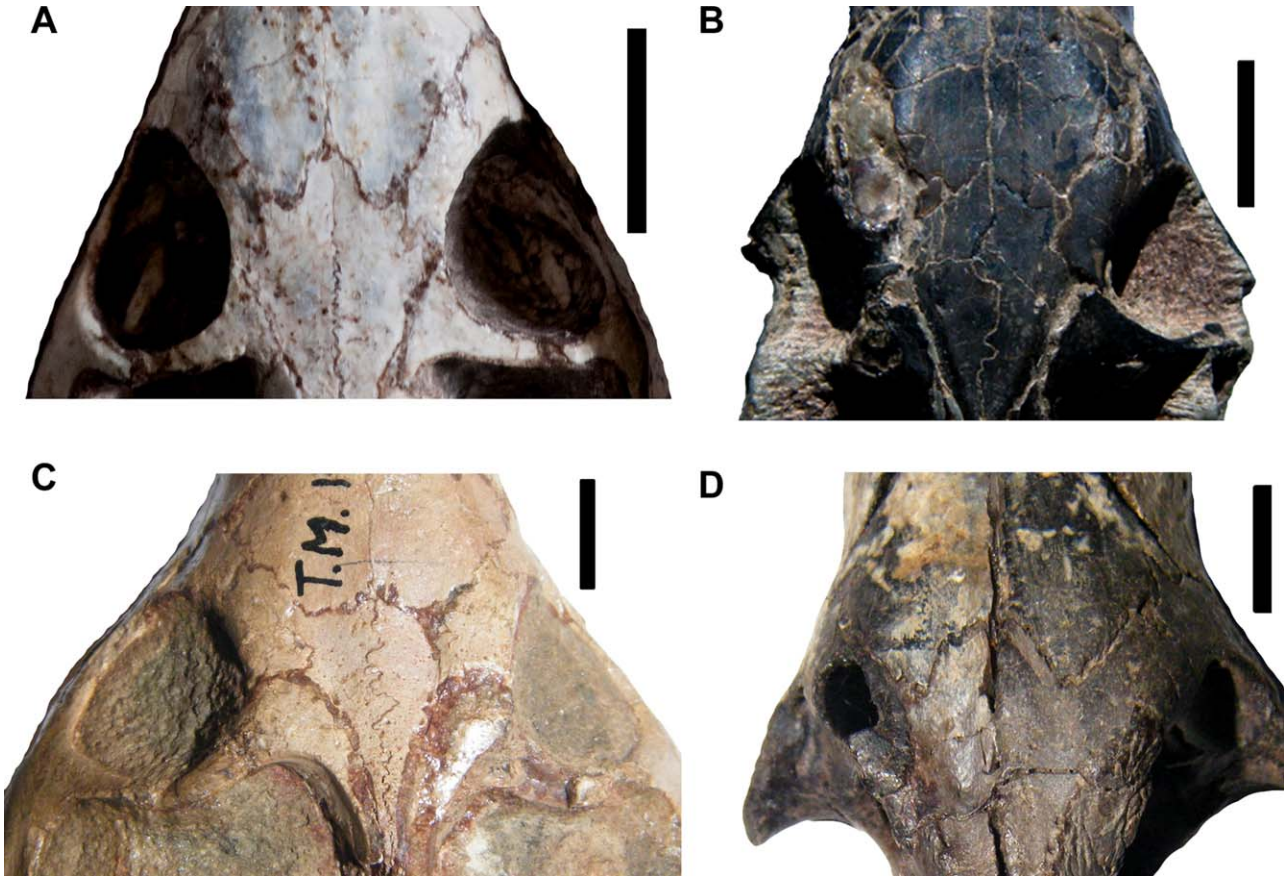

Fig. 5. *Thrinaxodon* skulls showing ontogenetic variation of the nasal-frontal suture: (**A**) inverted V-shaped in a juvenile (SAM-PK-K10017a); (**B**) an intermediate morphology between inverted V-shaped and transverse in a subadult (BP/1/4280); (**C**) transverse in an adult (TM 167); (**D**) rare, inverted V-shaped suture in an adult (TM 5074). Scale bars 10 mm.

parasphenoid forming a median crest (Fig. 8C). Estes (1961) indicated that there are remnants of the vacuities in UCMP 40466 (BSL = 74 mm); however this area is constricted, therefore it is unlikely that remnants of the vacuities remain.

Skull Roof

Frontal-parietal suture on surface. In our survey, we observed variation in the frontal-parietal suture on the dorsal surface of the skull roof (Fig. 9). In the small specimens SAM-PK-K8004 and BP/1/5372 (BSL $\leq$ 37 mm; Table 6), the frontals project posteriorly near the midline of the skull, whereas laterally the parietals project anteriorly, forming an M-shaped interdigitated suture (Fig. 9A; note that SAM-PK-K8004 has an irregularly shaped suture on the right side). In specimens with a BSL of ~39–42 mm (Table 2), the suture between the parietal and frontal is more transversely oriented (Fig. 9B; Estes, 1961: fig. 1). In specimens with a BSL of 56 mm or greater (Table 2), the suture between these bones becomes interdigitated, once again forming a M-shaped suture (Fig. 9C). With the development of a narrow (sharp) anterior parietal crest, the nature of the suture becomes obscured, but we assume that the suture remains interdigitated.

Postorbital bar. Brink (1955) stated that postorbital bar, formed by the postorbital bone dorsomedially and the jugal ventrolaterally, was incomplete in a small specimen of *Thrinaxodon* (BP/1/1376), which suggests that at the juvenile stage the bar was bridged midlength by a ligament. However, the postorbital bar was complete in all surveyed specimens that were well-preserved, including our smallest individuals (Table 2). It should be noted that at the midlength of the postorbital bar, the jugal and postorbital bones have an overlapping (scarf) contact that could easily disarticulate (e.g., BP/1/5372; Figs. 9A, 13A, 14A) or break after death. Therefore, the incomplete postorbital bar as reported by Brink (1955) was due to taphonomic processes rather than an ontogenetic feature of *Thrinaxodon*, and other ontogenetic studies have also confirmed this (e.g., van Heerden, 1972).

The postorbital bar is missing in several specimens, but the presence of a facet for its articulation with the skull roof indicates that it was lost after death. The taphonomic loss of the postorbital bar is attributed to the relatively flat scarf sutural connection between the postorbital bone and the skull roof. Because of the loose, overlapping contact between the postorbital and the frontal, prefrontal, and parietal bones (e.g., Fourie,

Fig. 6. Dorsal view of the skull of an adult *Thrinaxodon* (UCMP 42866). On the surface of the snout, the nasal-nasal suture is relatively straight with some interdigitations near the midlength of the snout (arrow) and the maxilla-nasal suture is scarf. Scale bar is 10 mm.

1974: figs. 15, 17) and the scarf suture with the jugal, there is a tendency for the postorbital bar to become disarticulated from the skull roof after death, sometimes exposing the facet on the skull roof (e.g., SAM-PK-K1498 and Figs. 5D, 11E). Movement of the postorbital bar out of its natural placement was observed in about a third of the specimens in our sample.

Posterior projection of the postorbital. van Heerden (1972) stated that length of the posterior projection of the postorbital, which overlaps the parietal on the lateral edge of the skull roof, changes during ontogeny. In young individuals, the projection is short, but in large specimens the projection extends halfway between the postorbital bar and parietal foramen (van Heerden, 1972). Our survey does indicate that the posterior postorbital projection is much shorter in smaller specimens (e.g., TM 80A; Fig. 10B) than in larger specimens (e.g., TM 180; Fig. 10C), in which the posterior margin of the projection is closer to the anterior edge of the parietal foramen.

We also observed that the shape of the posterior projection of the postorbital changes with age, a feature also noted by Sidor and Smith (2004). In the juvenile specimens that have well-preserved postorbital bars (TM 1486, BP/1/5372, and SAM-PK- specimens K10016, K10017a, and K10017b) there is a short (incipient) dorsally directed postorbital process and a much longer ventrally directed process that overlaps the parietal (Table 6; Fig. 10A).

In individuals larger than BSL of 56 mm, the posterior projection is clearly bifurcated producing a dorsal and ventral process that forms a distinctive C-shaped contact with the parietal (Fig. 10B,C). This thin postorbital projection often suffers from breakage, but in some specimens one can observe the facet for the process on the lateral surface of the parietal (e.g., TM 81a). In mechanically prepared specimens, the ventral posterior postorbital process is usually covered with matrix.

In a specimen of 67 mm DSL, Fourie (1974: fig. 6b) showed only a ventral process of the postorbital posterior projection. Our extensive sample shows that this condition is only found in young specimens (BSL $\leq$ 42 mm), therefore we think that the posterior projection of the postorbital was perhaps not completely preserved in his specimen.

Sagittal crest development. The development of the sagittal crest has been shown to vary ontogenetically by several studies (e.g., Estes, 1961; Sidor and Smith, 2004). The sagittal crest is mainly formed by the parietal bones, and partially by the interparietal posteriorly and the frontals anteriorly (the postorbitals also contribute to the crest in adult specimens). The progressive development of the sagittal crest was observed across the different ontogenetic stages of *Thrinaxodon*. The intertemporal region, both anterior and posterior to the parietal foramen, is dorsally flattened in the smallest juvenile specimen (SAM-PK-K8004; Fig. 11A). The paired temporal ridges, parallel and lateral to the midline of the intertemporal region, are more widely spaced anterior to the parietal foramen than they are posterior to the foramen (Fig. 11A). In the larger juveniles (BSL 33–40 mm, and SAM-PK-K10017b; Fig. 11B), the

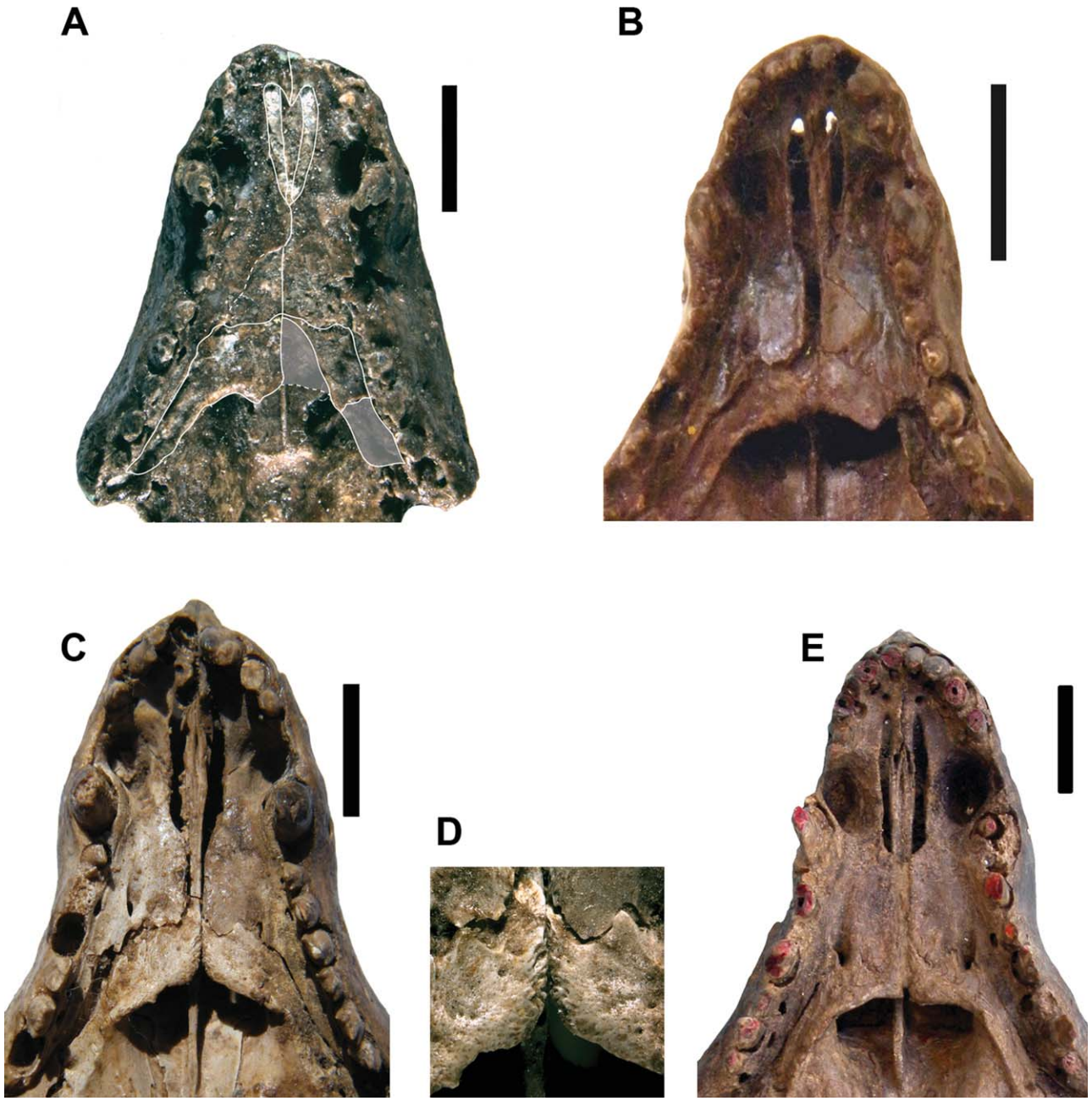

Fig. 7. The secondary palate remains open in all ontogenetic stages of *Thrinaxodon*. (**A**) BP/1/1376 (early juvenile with a distorted palate outlined in white); (**B**) TM 80A (subadult); (**C**) TM 81a (adult); (**D**) close-up of interpalatine rugosities in TM 81a; (**E**) NHMUK R511 (larger adult). Dashed lines and semi-transparent areas in (A) indicate broken bones. Scale bars are 10 mm.

posterior sagittal crest is still not developed but the temporal ridges have become narrower mediolaterally to form a flat posterior sagittal table. A sagittal crest began to form posterior to the parietal foramen in the juveniles with a BSL of at least 42 mm (SAM-PK-K10016, K10017a; Fig. 11C). In specimens with a BSL of 56–68 mm, the area anterior to the parietal foramen becomes narrowed to form an anterior sagittal table (Fig. 11D). The anterior part of the sagittal crest is developed in all specimens with a BSL of 69 mm or more (Table 2; Fig. 11E).

We examined a few juvenile specimens of similar size (BSL 40–42 mm; Table 2) to check qualitatively if there is a difference in sagittal crest development in young individuals. Specimens UCMP 42877 and SAM-PK-K10017b (Fig. 11B) differ from specimens SAM-PK-K10016 and -K10017a (Fig. 11C) in that they do not have a posterior sagittal crest but a narrow, flat sagittal table.

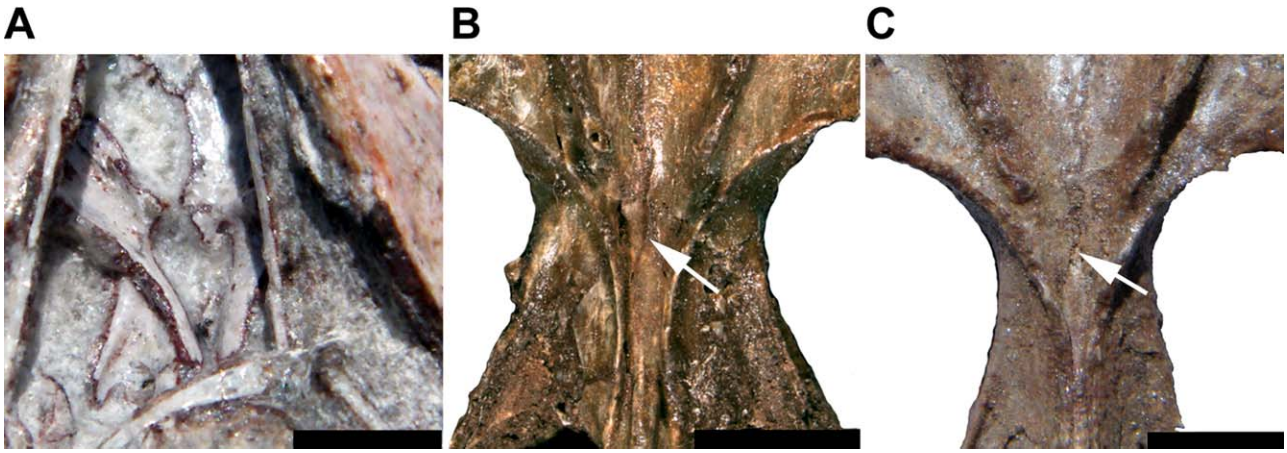

Fig. 8. Ventral view of the posterior palate and basicranial girder across different ontogenetic stages of *Thrinaxodon*. (**A**) Paired interpterygoid vacuities in the early juvenile BP/1/5372 (cultriform process is broken or distorted); (**B**) Infilling of bone in this area occurred in TM 80A (subadult); (**C**) TM 180 (adult) showing constriction of this area. Arrow indicates the anterior tip of the cultriform process. Scale bars are 5 mm.

We also checked the sagittal crest development in ten adult specimens of approximately 70–80 mm in BSL, all with well-preserved crests (Table 2: UCMP 42866, NHMUK R3731, SAM-PK-K1498, BP/1/5208, UCMP 40466, BP/1/2776, BP/1/7199, TM 180, TM K377, and NHMUK R5480). The sagittal crest is similar in the majority of specimens; however the crest anterior to the parietal foramen is slightly wider (width is similar to or greater than the width of the parietal foramen) in two specimens (TM K377, UCMP 42866).

Parietal foramen. As noted by Estes (1961), we also observed changes in the shape of the parietal foramen across the different ontogenetic stages. The change in shape appears to be related to the amount of development of the sagittal crest (see the section above), which was also noted by van Heerden (1972). The parietal foramen changes in shape from ovoid (transversely wide) in early juveniles (e.g., SAM-PK-K8004; Fig. 11A) to circular in slightly larger juveniles (e.g., SAM-PK-K10549) to ellipsoid (transversely narrow and anteroposteriorly long) in specimens with a posterior sagittal crest (e.g., SAM-PK-K10017a; Fig. 11C; Table 6).

Parietal-parietal suture. Posterior to the parietal foramen, the parietal-parietal suture is present in both immature and mature specimens. In the smallest specimen (SAM-PK-K8004; Table 2; Fig. 2A), the posterior parietal-parietal suture is not visible on the dorsal surface of the skull roof, but there are some irregular bony deposits in this area. In the micro-CT coronal sections of the juvenile specimen BP/1/5372, the posterior parietal-parietal suture is present for most of the depth of the skull roof, but near the dorsal (ectocranial) surface new bone has been deposited over the suture (Fig. 12A). In the intermediate-sized specimen TM 80A that has a posterior sagittal crest, the suture is visible only in the ventral half of the skull roof (Fig. 12B). In the three adult specimens that have a well-developed posterior sagittal crest (BP/1/7199, TM 180, SAM-PK-K378), the suture is present only near the ventral (endocranial) edge of the skull roof (Fig. 12C). The resolution is poor in the largest micro-CT specimen, BP/1/5905; however, an adult of similar size (BSL = 88 mm) illustrated by Broom (1938: fig. 2, section 14) shows that the posterior parietal-parietal suture remains patent near its ventral surface. It is not known if the suture is completely fused in the largest *Thrinaxodon* specimens (BSL = 96 mm).

Fig. 9. Ontogenetic variation in the frontal-parietal suture on the surface of the skull roof. (**A**), BP/1/5372 (M-shaped suture in an early juvenile); (**B**) SAM-PK-K10016 (transverse suture in a late juvenile); (**C**), BP/1/4280 (M-shaped suture in a subadult). Scale bars 5 mm.

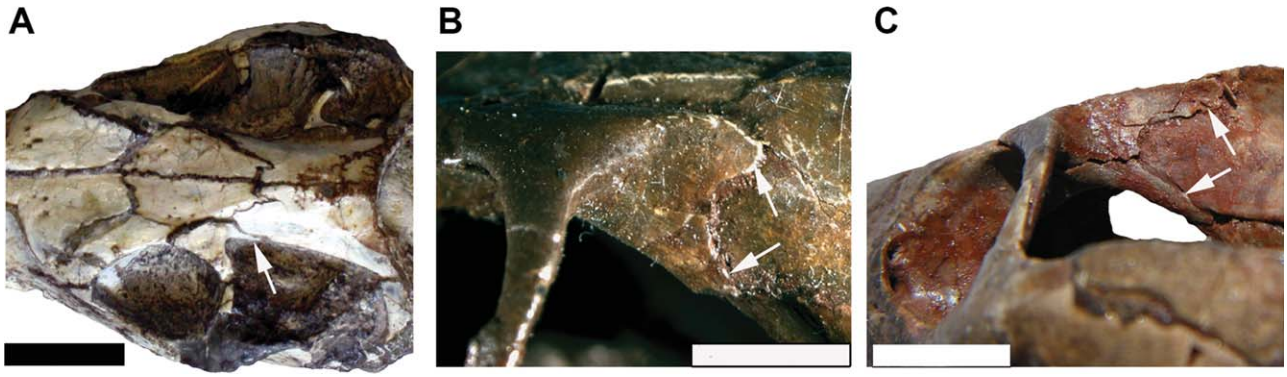

Fig. 10. Ontogenetic differences in the posterior projection of the postorbital. (**A**) In juvenile specimens (SAM-PK-K10016, dorsal view), the posterior postorbital projection is short and consists of a long ventral process (arrow) and an incipient dorsal process. (**B**) In specimens with a BSL larger than 56 mm (TM 80A, lateral view) the dorsal and ventral processes (arrows) are well-developed and form a distinctive "C." (**C**) In the older individuals, such as TM 180 (lateral view of right side, mirrored), the posterior projection of the postorbital (arrows) becomes longer. Scale bars for (A) and (C) is 10 mm; scale bar for (B) is 5 mm.

Therefore the posterior parietal-parietal suture does not appear to fuse during growth. Instead, new bone was deposited dorsally over the suture (ectocranial apposition) to form a unified posterior sagittal crest, and the ventrally positioned suture was retained in all ontogenetic stages (Fig. 12).

The only exception to this observation was reported by Fourie (1974), in which he indicated that the posterior parietal-parietal suture was completely fused in specimen NM C354 (Fourie, 1974: p. 375; figs. 19, 20). We cannot independently verify his observation because he did not photograph the original sections that were ground away (destroyed). However, the intermediate size of the specimen (DSL 67 mm) suggests that the suture should be present along the ventral part of the skull roof.

In contrast, the parietal-parietal suture anterior to the parietal foramen spanned the entire depth of the parietal skull roof in all ontogenetic stages that were investigated with micro-CT (Table 2). This observation is corroborated by Broom's serial-sectioned large adult specimen (1938: fig. 2, section 13); however, Fourie (1974) did not illustrate or state the nature of the anterior part of the suture in NM C354. In our smallest *Thrinaxodon* specimen (SAM-PK-K8004; Table 2; Fig. 2A), the anterior parietal-parietal suture appears patent on the surface of the skull.

Interparietal suture. Estes (1961) stated that the interparietal (=dermosupraoccipital) is paired in the juveniles UCMP 42877 and 42878, whereas in adults the bone is fused. No other study has corroborated the presence of an interparietal suture in other small specimens of *Thrinaxodon*, and we were unable to confirm Estes' observation from digital photographs of the UCMP specimens. The micro-CT scans of BP/1/5372, a juvenile specimen of similar size (Table 2), and of a larger specimen TM 80A, did not show any indications of a midline suture through the interparietal.

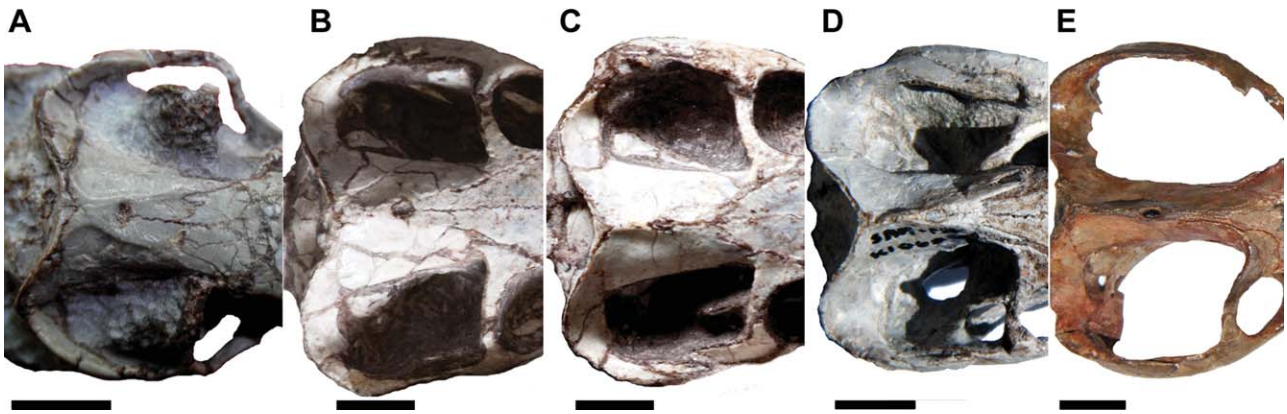

Fig. 11. Ontogenetic variation in the development of the sagittal crest and parietal foramen. (**A**) SAM-PK-K8004 (no sagittal crest development in the early juvenile stage, but temporal ridges are present); (**B**) SAM-PK-K10017b (posterior sagittal table in a late juvenile); (**C**) SAM-PK-K10017a (posterior sagittal crest developed in a late juvenile); (**D**) SAM-PK-K10607 (anterior sagittal table in the subadult stage); (**E**) TM 180 (both the anterior and posterior sagittal crest is developed at the adult stage). Scale bar for (A-C) is 5 mm, scale bar for (D-E) is 10 mm.

Basicranium

Unossified region: basioccipital-basisphenoid. The unossified region between the basioccipital and basisphenoid cannot be recognized externally, therefore the only way to access this zone is by physically sectioning or virtually slicing the skull. This unossified zone was previously observed in three specimens with a skull length of 67–74 mm (Olson, 1944; Fourie, 1974; Rowe et al., 1993). An unossified zone was noted by Estes (1961: 169) in the gross ventral view of a juvenile specimen (UCMP 42877); however, after examination of the specimen we were unable to recognize it. Estes also described a small unossified gap between basioccipital and basisphenoid in the intermediate-sized specimen UCMP 42865. From Estes' (1961: 173) description of this specimen, it appears that he sectioned the basicranium of UCMP 42865 although he did not illustrate or explicitly state this in his study.

Our observations of micro-CT scanned *Thrinaxodon* specimens indicate that the unossified region occurs in both immature (BP/1/5372, TM 80A) and mature (BP/1/7199, TM 180, BP/1/5905) specimens (Table 2), therefore it does not provide evidence for ontogenetic change. However, it does suggest that growth of the skull is sustained during the entire life of the individual.

Parasphenoid teeth. Estes (1961) described the presence of teeth on the parasphenoid of a juvenile specimen of *Thrinaxodon* (UCMP 42877). As mentioned by Estes (1961), this area is rough, and F. Abdala observed tiny projections in that area. However, small projections were not observed on the parasphenoid in any other specimen of our large sample of *Thrinaxodon*. Parasphenoidal teeth are not known to occur in therapsids, but are found in some non-therapsid synapsids, that is, "pelycosaurs" (Langston and Reisz, 1981; Anderson and Reisz, 2004). Therefore we interpret these parasphenoid projections in UCMP 42877 as a result of a broken bone surface rather than teeth.

Zygoma

Angulation of the zygomatic arch. The angulation of the zygomatic arch is defined as the presence of a distinct angle between the posteroventral edge of the maxilla and the anteroventral portion of the jugal below the orbit. This feature has been documented in three adult epicynodont taxa (Fig. 1): *Galesaurus* (Abdala, 2003; Abdala and Damiani, 2004), *Progalesaurus*, and *Platycraniellus* (Abdala, 2007). In the current survey, angulation of the zygomatic arch was found only in two large adult individuals of *Thrinaxodon* (BP/1/2824, NMQR 809), which have a BSL of ~90 to 91 mm (Table 2; Fig. 13A). Angulation of the zygomatic arch was not found in any of the smaller or immature *Thrinaxodon* specimens, or in specimens NMQR 1864, USNM 22812, and SAM-PK-K1461 that have a BSL greater than 90 mm and a well-preserved zygomatic arch (Table 2; Fig. 13B). The presence of the angulation of the zygomatic arch of *Thrinaxodon* appears to be a result of intraspecific variation rather than ontogenetic change.

Occiput and Braincase

van Heerden (1972) proposed that the occiput of *Thrinaxodon* became more vertical in orientation with

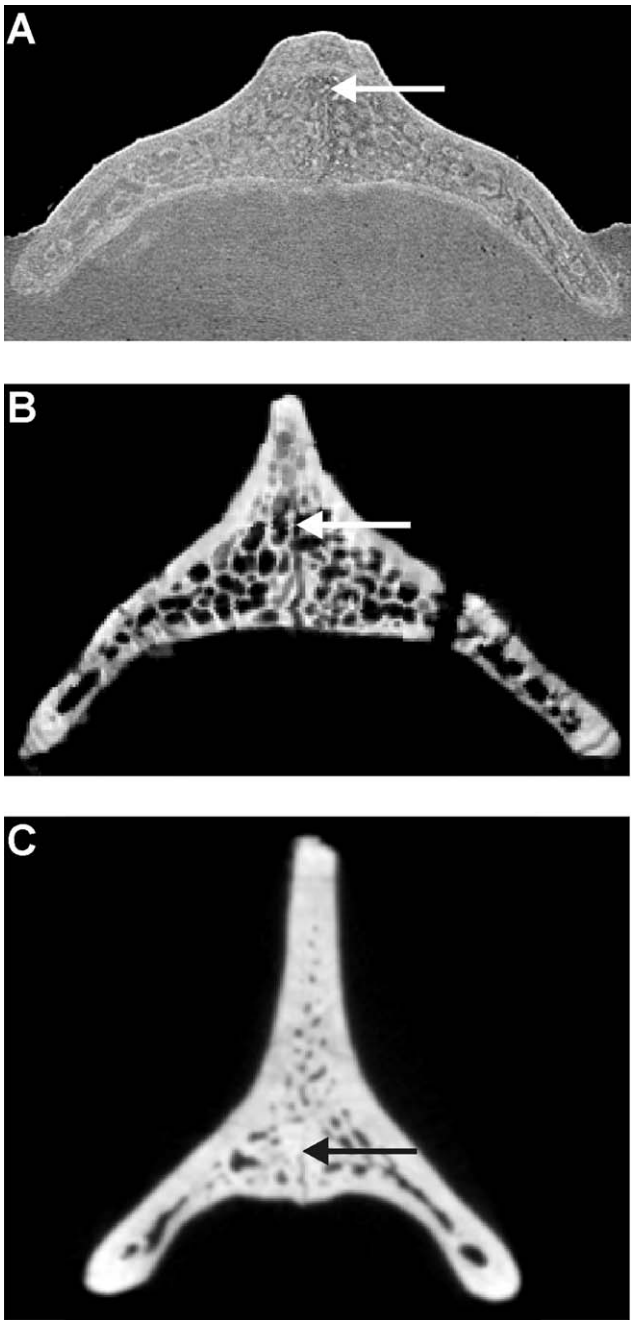

Fig. 12. Coronal micro-CT slices through the posterior intertemporal region of three ontogenetic stages of *Thrinaxodon* showing the progressive deposition of bone onto the dorsal edge of the parietals and the retention of the posterior parietal-parietal suture ventrally. (**A**) In the early juvenile BP/1/5372, there is no posterior sagittal crest and the parietal-parietal suture extends close to the dorsal edge of the parietal bones. (**B**) In the subadult TM 80A, bone has been deposited dorsally to form the posterior sagittal crest, and the parietal-parietal suture is present along the ventral half of the parietal bones. (**C**) In the adult TM 180, additional bone has been deposited dorsally to form a tall posterior sagittal crest, and the parietal-parietal suture is present only near the ventral edge of the parietal bones. Arrow indicates the approximate dorsal-most position of the posterior parietal-parietal suture. See Table 2 for specimen sizes.

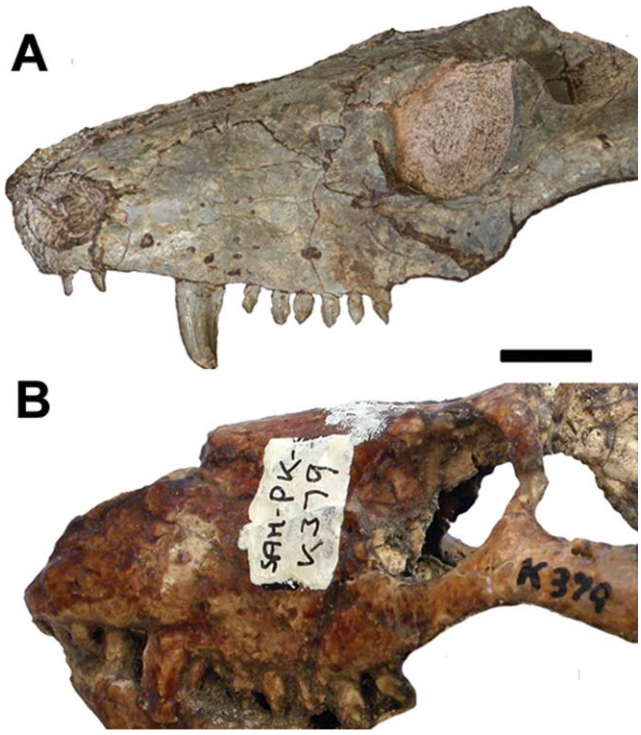

Fig. 13. Variation in the presence of angulation of the zygomatic arch in large adult specimens of *Thrinaxodon*. (**A**) Angulation of the zygomatic arch is present in BP/1/2824 (image is mirrored), whereas it is absent from (**B**) SAM-PK-K379, a similar-sized adult specimen. Scale bar is 10 mm.

age and that the squamosal-tabular-parietal complex (which includes the lambdoidal [nuchal] crest that runs transversely along the posterior edge of the temporal fenestra) became dorsally and posteriorly extended. Our survey indicated that the angle of orientation of the occiput does not change, but we confirmed that the lambdoidal crest becomes more developed and projects further posteriorly over the occiput, making the whole structure appear more vertical. We also observed in specimens with a BSL of 56 mm or less (Table 2) that the supraoccipital is bulbous and projects further posterior than the occipital condyle. In specimens with a 61 mm BSL or greater (Table 6), the occipital condyle protrudes further posteriorly and the supraoccipital becomes less bulbous.

A low external occipital crest (= median nuchal line) along the midline of the interparietal on the occiput was observed in most specimens with a BSL of at least 61 mm, but was absent from smaller specimens (Table 2). It should be noted that the occiput in several large specimens (BSL > 85 mm) was not fully prepared or it was deformed, making it difficult to determine the presence of this feature. In the specimens that had a well-preserved occiput, we observed some variation in the presence and development of the external occipital crest. Five specimens with a BSL of 61 mm or greater lacked an external occipital crest. When present, the crest varied from a low swelling to a low, sharp ridge, but in general it is poorly developed. The external occipital crest extends ventrally onto the supraoccipital in only a few adult specimens.

Although the width of the braincase was not included in the bivariate analysis, qualitative observations indicate that this variable would be strongly negative allometric. For example, the braincase width is very similar between the early juvenile SAM-PK-K10549 (BSL ~39 mm; braincase width 7.7 mm) and the large adult NMQR 810 (BSL 96 mm; braincase width 8.6 mm), with the adult having a slightly wider braincase by only 0.9 mm.

DISCUSSION

Cranial Allometry in *Thrinaxodon liorhinus*

Allometric trends in *Thrinaxodon* were found in the variables related to the orbit, snout, palate, and temporal region of the skull. The general model of skull change in *Thrinaxodon* is as follows: a slower growth rate for the orbit (OD, OL) and posterior part of the palate (PD), and a faster growth rate in the length of the snout (MUL), palate (PAL), and temporal region (MTO, TEL, POP, and PSC) (Table 3). Negative allometry of the orbital region is a common trend observed in tetrapods. Positive allometry of the MUL and PAL indicate that the snout is growing relatively faster, possibly to accommodate the larger size of the postcanine teeth and the posterior migration of the postcanine tooth row (see Abdala et al., 2013). The variables MTO and TEL show positive allometry (Fig. 4A) indicating that the temporal region including the sagittal crest in adults is relatively more developed than in juveniles, whereas the width of the temporal fenestrae (a measure indicated by SW) has slower growth (isometric with RMA and negatively allometric with LS; Table 3; Fig. 4B).

Parrington (1936) analyzed changes in the skull proportions across several specimens of *Thrinaxodon*. In dorsal view, Parrington (1936: fig. 3) aligned six specimens [from smallest to largest: B, UMZC T812 (=R2739); C, UMZC T813 (=R2737); E, NHMUK R3731; F, UMZC T815 (=R2734); G, NHMUK R5480; H, UMZC T816 (=R2736)] (Table 1) according to the location of the parietal foramen. Parrington (1936: fig. 3) graphically indicated that the snout and the area posterior to the parietal foramen of *Thrinaxodon* increased during ontogeny, but that the snout increased to a greater degree than the posterior skull roof. He also calculated ratios of the lengths of three different segments of the skull between the smallest and largest specimens. His calculations indicated the increase in the length of the snout was the largest (42%), followed by the region between the parietal foramen and the anterior margin of the orbits (35%), and then by the region between the parietal foramen and the posterior extent of the sagittal crest (23%). Parrington (1936) also indicated a faster growth rate for the width of the skull (a 50% increase) in comparison to the length (35%). In lateral view, Parrington (1936: fig. 4) compared three relatively undistorted specimens (C, UMZC T813; F, UMZC T815; H, UMZC T816) and found similar changes in proportions as in his figure 3.

Contrary to Parrington's (1936) conclusions, our results indicate that the temporal region grew faster in length than the snout (Table 3). The region between the parietal foramen and the posterior extent of the sagittal crest shows a strong positive allometry, whereas the snout also has a positive allometry but the coefficient of allometry (1.17) is much lower than those of the temporal region (1.40, 1.42, and 1.48; Table 3). In addition, our bivariate analysis comparing BSL and SW shows that the width

has isometric or negative growth and is therefore growing at the same or a slower rate relative to skull length.

From a sample of 22 *Thrinaxodon* specimens (Table 1), van Heerden (1972) also presented ratios of four measurements relative to dorsal skull length: snout length, anterior margin of the orbit to middle of the parietal foramen, middle of parietal foramen to the back of the sagittal crest, and total width of the skull at the level of the parietal foramen. The first and the last measurements are directly comparable to our variables (MUL and SW, respectively), the third measurement is similar to our PSC (Fig. 3A), whereas the second variable is a combination of the length of the orbit and anterior temporal region and is therefore not comparable to our results. van Heerden (1972) took the average ratio between each variable and the dorsal skull length from five groups of individuals, and it appears he then calculated a regression line through these average ratios. Regarding snout length, van Heerden (1972: graph 1) suggested that negative allometry occurred in smaller specimens (<50 mm of skull length), whereas the trend was isometric in specimens larger than 50 mm. Our bivariate results, however, indicate positive allometry for this variable (Table 3). Regarding the SW, graph 4 showed that "there was a *progressive relative increase* in skull width during growth" (van Heerden, 1972: 341). van Heerden (1972) also interpreted for this graph two subsamples that he considered represented sexual dimorphism, with the males presumably having the wider skull due to increased development of the temporalis musculature. However, our bivariate analysis indicates that skull width increases isometrically or with negative allometry (Table 3; Fig. 4B). van Heerden (1972: graph 3) found that the posterior part of the temporal region increased at a faster rate than the length of the skull, which is consistent with our results (PSC, Table 3).

Although van Heerden (1972) did not include the height of the zygomatic arch in his larger quantitative study, he measured this variable in two specimens, NMQR 24 and NMQR 809 (Table 1), as part his qualitative observations (p. 314). He determined there was an increase in relative height in the arch in the larger specimen NMQR 809. However, our comprehensive bivariate study found that zygomatic height is isometric (Table 3), which may indicate that the masseter muscles that originated from the zygomatic arch did not increase more rapidly with age.

A RMA analysis was then conducted using the data presented by van Heerden (1972: table 7). This new analysis resulted in the snout length being positively allometric ($b = 1.09$; $p = 0.02$) and the SW being isometric ($b = 1.0$; $p = 0.89$). These trends are similar to that obtained from our extensive dataset, with MUL being positive ($b = 1.17$; $p = 2.40\text{E-}05$) and SW being isometric ($b = 0.95$; $p = 0.28$, under RMA) (Table 3). In addition, van Heerden's (1972) measurement from the middle of the parietal foramen to the posterior extent of the sagittal crest, a variable related to the intertemporal region, has a strong positive allometry ($b = 1.36$; $p = 0.0001$). The PSC in our dataset also showed positive allometry ($b = 1.49$; $p = 3.50\text{E-}05$) (Table 3) but the values are relatively higher.

Comparative allometry in non-mammaliaform cynodonts. Cranial allometry has been investigated in only a few other non-mammaliaform cynodonts, including *Diademodon tetragonus* (Grine and Hahn, 1978; Grine et al., 1978; Bradu and Grine, 1979), *Massetognathus pascuali* (Abdala and Giannini, 2000), and *Chiniquodon theotonicus* (Abdala and Giannini, 2002) (Tables 4, 5; Fig. 1). Therefore, it is important that the allometric results from *Thrinaxodon* are compared to these previous studies.

The first interesting point of comparison is that *Massetognathus pascuali*, which also has a good sample size (*n* varies between 16 and 31; Abdala and Gianinni, 2000; Table 4), has nearly the same number of variables that depart from isometry in comparison to those of *Thrinaxodon* (11 in *M. pascuali* versus nine in *T. liorhinus*; Table 5). In *Chiniquodon* and *Diademodon*, there are six and five variables, respectively, that depart from isometry (Table 5).

The growth models among these cynodont species, however, are quite different as there are opposite trends for some variables. The positive allometry of TEL is shared by the sectorial toothed cynodonts *T. liorhinus* and *C. theotonicus* and also by the traversodontid *M. pascuali* (Table 5; no values for *D. tetragonus*), which shows that the lengthening of the temporal region is a ubiquitous cranial change during ontogeny and indicates a well-developed temporalis musculature. An expected common trend is the negative allometry in the OD in *T. liorhinus*, *M. pascuali* and *D. tetragonus* (no coefficient reported for *C. theotonicus*). The only remaining shared allometric variable of *T. liorhinus* is a negative one for the OL, which is also observed in *M. pascuali*; however, this variable is isometric in *C. theotonicus*.

The SW in *T. liorhinus* has an isometric or negative trend, which is unlike any of the three eucynodonts that show positive allometry for this feature (Table 5; it is marginally significant for *Diademodon*). This may be explained by the fact that the zygoma in *T. liorhinus* is less flared laterally than in the other three species. Isometric trends in the maximum width of the skull were also reported in small to medium-sized extant marsupials such as *Didelphis albiventris* and *Dromiciops gliroides* where the expansion of the temporal fenestrae was a consequence of the interaction between the isometry of the skull width and the negative allometry of the braincase (Abdala et al., 2001; Giannini et al., 2004). This suggests that the temporal fenestra expanded medially to accommodate the further development of the adductor musculature during growth; however, the relative reduction in braincase width is much more extreme in extant mammals than in *Thrinaxodon*. The height of the zygomatic arch is isometric in *T. liorhinus*, whereas it is positively allometric in the three eucynodonts (Table 5). In addition, the zygomatic arch is more robust in these eucynodonts in comparison to that of *Thrinaxodon*, suggesting that the masseter muscles were less developed in *Thrinaxodon*.

Bicanine width (BW) is isometric in the herbivorous/omnivorous *M. pascuali* and *D. tetragonus* as it is in *T. liorhinus* but has a positive allometry in the large sized carnivorous *C. theotonicus* (Table 5). This is consistent with the enormous development of the canine prominence on the lateral edge of the chiniquodontid snout. The PD has a negative allometry in *Thrinaxodon* and *Massetognathus*, whereas it is isometric in *Chiniquodon*.

Qualitative Differences During Ontogeny

Nasal-frontal suture. Overall it appears that Estes (1961) was correct to assume that the shape of the nasal-frontal suture can be used as an ontogenetic feature, even though there is some individual variation of the suture morphology. Estes (1961), citing the putative absence of frontal spines in Brink's (1955: fig. 26a) juvenile specimen (BP/1/1376), also stated that the nasal-frontal suture can be a variable trait in juveniles. However, van Heerden (1972) stated that the variation in the ectocranial suture morphology across different-sized specimens is due to individual (intraspecific) growth patterns and perhaps ontogenetic change. Both of these studies considered only a few specimens of *Thrinaxodon* (Table 1). Our larger survey that took into account individual variation indicated that the shape of the nasal-frontal suture can be used, although with some caveats, to distinguish between different-sized individuals (Fig. 5; Table 6).

Secondary palate. Although the secondary palate of *Thrinaxodon* is often illustrated as being completely closed (e.g., Parrington, 1946: fig. 2; Estes, 1961: fig. 2), our study found that the secondary palate remained open in all ontogenetic stages of *Thrinaxodon*. Parrington's (1946) description of *Thrinaxodon* stated "The *palatines*, where they contribute to the formation of the false palate, **almost hide** the anterior borders of the horizontal component of the vomer" (Parrington, 1946: 183; bold text is ours). We interpret from his description that there was a small gap present between the palatines, which is in contrast to his figure that showed a closed palate (Parrington, 1946: fig. 2). Parrington's figure (1946: fig. 2), which appears to be a composite of multiple specimens, has been reproduced several times (Barghusen, 1986: fig. 1B; Carroll, 1988: fig. 17.32b; Allin and Hopson, 1992: fig. 28.5E; Kemp, 2005: fig. 3.20a), and has reinforced the idea that the secondary palate of *Thrinaxodon* is closed and hides the fact that there is variation in this feature.

Our survey shows that the palatal shelves (intermaxillary and interpalatine) do not contact each other at the midline of the secondary palate in undistorted specimens of *Thrinaxodon* of all ages (Fig. 7). The openness of the *Thrinaxodon* secondary palate was also recently noted by van Heerden (1972), Fourie (1974: figs. 1, 8b, 9), and Abdala and Allinson (2005). The midline gap in the secondary palate of *Thrinaxodon* was most likely bridged by extensive fibrous soft tissue. Fourie (1974) suggested that a bridge of strong connective tissue ran across the maxilla-palatine cleft, attaching to the dorsal ridge of maxilla and palatine bones, and the ventral edge of the vomer.

From our survey of *Thrinaxodon* specimens, the palatines appear to be closer together than the maxillae, suggesting that in a later evolutionary stage the palate would close in the posterior to anterior direction. However, in modern mammals the palate fuses in the anterior to posterior direction (e.g., Tonge and Luke, 1985; Wang et al., 2006). Thus, the morphological changes that we see in *Thrinaxodon* do not match the developmental closure of the sutures in modern mammals.

In comparison to other cynodonts, the openness of the *Thrinaxodon* palate is not as extreme as in *Procynosuchus* and *Cynosaurus* (Fig. 1). In these basal cynodonts, the palate is starting to close (Thomason and Russell, 1986) but the maxilla-palatine cleft is much larger than in *Thrinaxodon*. The more derived *Thrinaxodon* falls within an intermediate stage between the basal cynodont condition and a completely closed secondary palate in Eucynodontia (Fig. 1). Thus, it can be expected that the condition of the secondary palate is variable at this evolutionary stage. Complete closure of the secondary palate in Eucynodontia would increase torsional strength of the snout (Thomason and Russell, 1986); however it is expected that a semi-closed palate with stiff sutural fibers bridging the midline gap in epicynodonts would also impart strength to the snout.

Interpterygoid vacuity. Paired interpterygoid vacuities are present in juvenile specimens of *Thrinaxodon*, but are absent from specimens with a BSL of 56 mm or larger (Table 6). Therefore this feature is an ontogenetic character of *Thrinaxodon*.

An interpterygoid vacuity is known in adults of Late Permian *Procynosuchus* and *Dvinia*, and Early Triassic *Platycraniellus*, whereas it is mostly absent from the remaining Late Permian and Early Triassic cynodont species (adult and juvenile specimens) in which the basicranial girder is known (Abdala, 2007; Botha et al., 2007; Fig. 1). This feature is also pervasive in therocephalians in which the vacuity seems to have an ontogenetic trend in at least *Theriognathus* (Huttenlocker and Abdala, in press). In addition, the vacuity is inordinately large in small-sized therocephalians (F. Abdala, pers. obs.) again suggesting ontogenetically related variation.

Estes (1961) suggested that the obliteration or loss of the interpterygoid vacuities in larger specimens is due to the greater development of the pterygoideus muscle, which would have put pressure on that region. The increase in muscle mass may have constricted the paired pterygoids in that region, forming the median pterygoid crest that is observed in larger specimens of *Thrinaxodon*. However, the infilling of the interpterygoid vacuities might not be fully explained by the increase in pterygoideus musculature.

More recently, Martinelli (2009) indicated that the area of the vacuity is an important connector of two cranial regions, and he interpreted it as a growth zone that will continue growing until late in ontogeny and allow the skull to increase in length and width. As mentioned by Martinelli (2009), the elongation of the skull at the basicranial girder is evident in *Massetognathus* (see Abdala and Giannini, 2000: fig. 5); a long and narrow basicranial girder is also a common condition observed in eucynodonts (e.g., *Cynognathus*, *Diademodon*; Fig. 1). We did not measure the basicranial girder length in *Thrinaxodon*, but visual inspection of juveniles and adults shows a lengthening of the girder accompanying the development of the temporal fenestra. As for the width, *Thrinaxodon* had isometric growth of the basicranial girder (BGW, Table 3).

Frontal-parietal suture. The morphology of the frontal-parietal suture, not previously mentioned in other ontogenetic studies of *Thrinaxodon*, appears to be an ontogenetic feature of this taxon. The three morphologies separate the specimens into early juvenile, late juvenile, and more mature individuals (including the

subadult TM 80A) (Table 6). The change in the external morphology of this suture is most likely due to the growth (extension) of the intertemporal skull roof.

Posterior projection of the postorbital. In juveniles (BSL $\leq$ 42 mm), the posterior projection of the postorbital consists of a long ventral process and an incipient dorsal process, but in older individuals (BSL $\geq$ 56 mm) the dorsal process becomes more developed and the posterior margin of the postorbital bone is C-shaped (Table 6). The lengthening of the posterior projection of the postorbital appears to coincide with the lengthening of the intertemporal skull roof in larger individuals.

The lengthening and bifurcation of the projection would allow increased contact between the postorbital and parietal bones in the intertemporal region. This increased lateral bony overlap could help stabilize the postorbital bar, which had a relatively loose connection with the dorsal edge of the skull roof. In addition, it could also help dissipate the increased temporal muscle stresses in the skull of more mature individuals, and possibly prevent deformation of the braincase (see Hopson's [1991] functional explanation for development of frontal and parietal ventrolateral flanges in cynodonts).

Sagittal crest development. The sagittal crest develops at different ontogenetic stages of *Thrinaxodon*: the posterior part of the sagittal crest first appears at 42 mm in BSL, whereas the anterior crest does not develop until specimens are at least 69 mm (Table 6). The progressive development of the sagittal crest is supported by the allometric study, which indicates strong positive allometry of TEL, POP, and PSC (Table 3). Not only does the posterior sagittal crest develop earlier in ontogeny, but the parietal bones progressively grow together to form the posterior sagittal crest (Fig. 12). This indicates that the posterior intertemporal region was strengthened with age because it formed a single unit in which only the ventral part of the structure had a patent suture.

In modern mammals, the development of the sagittal crest is related to the development of the temporalis musculature (e.g., Washburn, 1947; Wolpoff, 1974). In some of the mammals that develop sagittal crests, the cranial vault is smooth at the early juvenile stage, and during ontogeny temporal ridges (=temporal lines or parasagittal ridges) develop on either side of the midline (Garcia-Perea, 1996; Holbrook, 2002). These ridges then migrate medially and dorsally to form a sagittal table, or if the ridges coalesce, they form a sagittal crest (Holbrook, 2002). This developmental pathway of the sagittal crest is similar to that observed in *Thrinaxodon*, although temporal ridges were already present in the early juvenile specimens of *Thrinaxodon* (Fig. 11A). In a few extant mammals, such as the marsupials *Dasyurus albopunctatus* and *Didelphis albiventris* (Abdala et al., 2001; Flores et al., 2006; F. Abdala, pers. obs.) and the tapir *Tapirus terrestris* (Holbrook, 2002), the sagittal crest appears suddenly without the migration of temporal ridges. In the last taxon, the sudden appearance of the sagittal crest in juveniles may be due to the strong development of the temporalis musculature at an early age (Holbrook, 2002).

There is, however, some variation in the timing of the development of the sagittal crest in *Thrinaxodon*. This variation in the development in young, similar-sized individuals found in close association (SAM-PK-K10017a and -K10017b; Table 2; Fig. 11B,C) might be explained by two possibilities: (1) variability in the timing of the initial development (individual variation) or (2) sexual dimorphism. This difference is not expressed in later stages of ontogeny and therefore most likely indicates individual variation rather than sexual dimorphism. This is supported by the survey of 10 similar-sized adults of this species that showed there are no obvious differences in the structure of the sagittal crest, suggesting that the crest of adult *Thrinaxodon* does not exhibit sexual dimorphism.

The temporalis muscle in *Thrinaxodon* originated from an aponeurosis that covered the temporal fenestra (attaching to the edges of the parietal, squamosal, and postorbital bones) and from the surface of those bones; it inserted onto the coronoid process of the mandible (Barghusen, 1968, 1972). Evidence for this aponeurotic origin is provided by the presence of a continuous sharp edge along the margins of the postorbital bone, intertemporal region (temporal ridges), and the lambdoidal crest in most specimens irrespective of whether the sagittal crest was developed or not.

The origin of the temporalis from the sagittal crest was affected by growth. The earlier appearance of the posterior sagittal crest in the ontogeny of *Thrinaxodon* (Table 6) suggests that the posterior fibres of the temporalis muscle developed sooner and to a greater extent than the more anterior fibres. On the contrary, the later appearance of the anterior sagittal crest in the adult stage (Table 6) and the scarf contact between the postorbital bar and skull roof suggests that the anterior origin may not have been as developed as the origin from the posterior intertemporal region. The temporal region (TEL, MTO) scales with positive allometry suggesting the volume of the temporalis would have greatly increased with age. Associated with this is the presumed negative allometry of the braincase in adults (estimated from qualitative observations that the braincase becomes relatively narrower in adults), which would have somewhat contributed to the enlargement of the temporal fenestra.

In contrast, the nature of the insertion of the temporalis onto the coronoid process does not appear to vary with age. A comparison of the mandible of three micro-CT specimens (BP/1/5372, BP/1/7199, BP/1/5905; Table 2) indicates that the coronoid process does not greatly differ in shape or relative height (Fig. 14). This trend of apparent isometry of the coronoid process is also seen in several modern carnivoran taxa (Emerson and Bramble, 1993).

The early juveniles of *Thrinaxodon*, which lacked a sagittal crest, may have had a different cranial function, perhaps eating different food items compared with more mature individuals. The ratio of the relative length of the in-lever of the temporalis compared to the out-lever length (distance to the bite point to the first premaxillary incisor) is similar between the early juvenile and adult ontogenetic stages (Fig. 14), indicating that the mechanical advantage (bite force and speed) is similar.

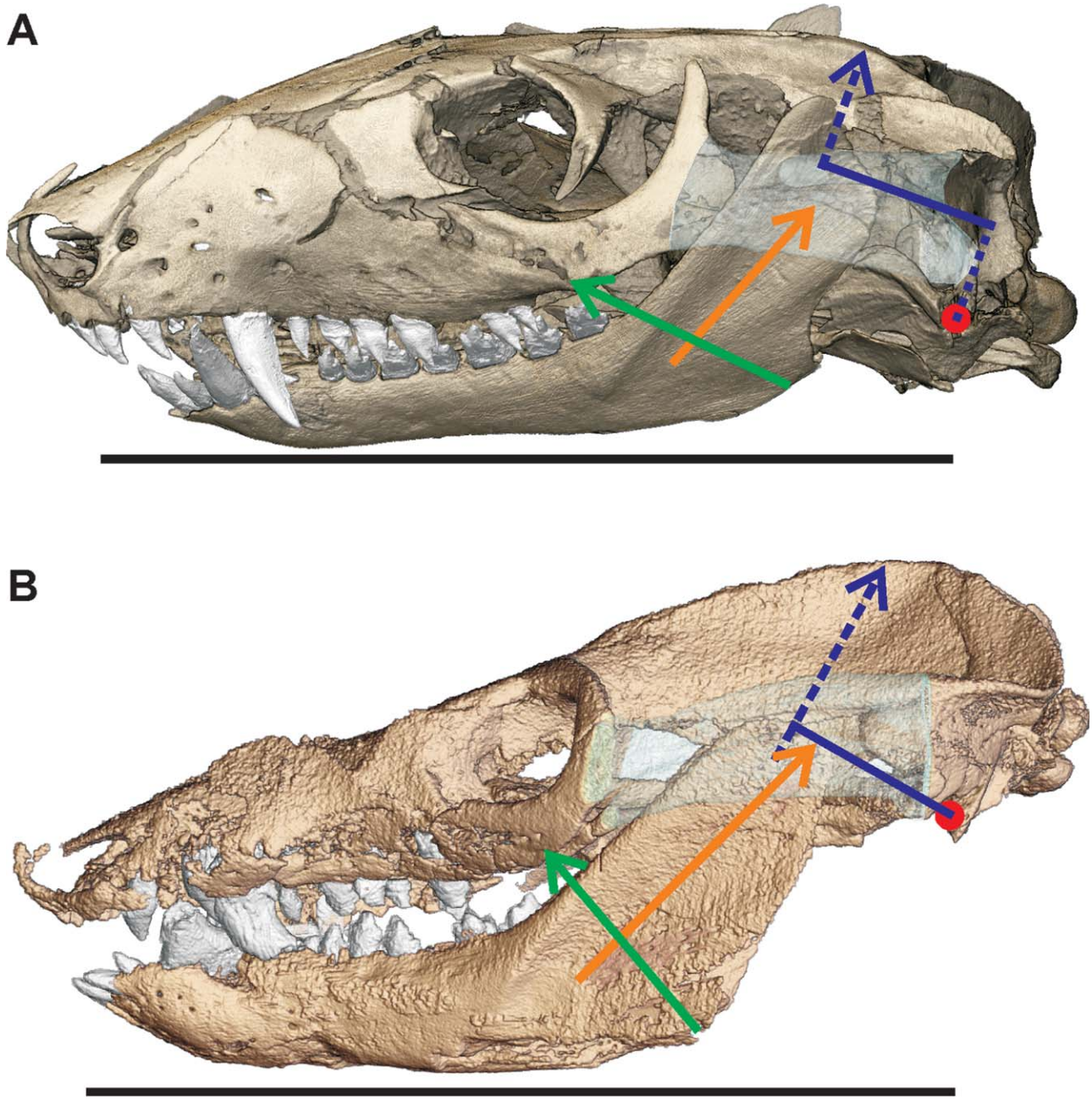

Fig. 14. Three-dimensional segmentation of the skull and mandible of *Thrinaxodon*. (**A**) The early juvenile specimen BP/1/5372; (**B**) the large adult specimen BP/1/5905 (postdentary bones not shown). The zygomatic arch is semitransparent in both models to show the coronoid process. Note that the vertical position of the mandible relative to the skull differs slightly between the two specimens. Superimposed on each model is the in-lever (solid blue line) of the temporalis muscle (blue dashed arrow) and the out-lever (black line; distance to the bite point which is the first premaxillary incisor). The orange and green arrows represent the line of action of the deep and superficial masseter muscles, respectively. Both models are scaled to the same skull length and aligned to the quadrate (red dot); see Table 2 for BSL. Note that the length of the in-lever of the temporalis is similar in both specimens, but that the point of origin from the sagittal crest is much higher in the adult than in the early juvenile.

However, the increase in the height of the sagittal crest would have increased the area for muscle attachment, and perhaps increased the bite force [see the study by Herrel et al. (2002) of head height and biting performance in turtles]. Even though there was an increase in muscle volume, as indicated by the larger MTO in adults (Table 3) and an increase in sagittal crest height, the relative height and size of the coronoid process did not vary much with age (Fig. 14).

Parietal-parietal suture. In *Thrinaxodon* there is a distinct difference between the posterior parietal-parietal suture and the portion anterior to the parietal foramen. Both sutures are retained across all

ontogenetic stages, but the anterior parietal-parietal suture spanned the entire depth of the skull roof, whereas the posterior parietal-parietal suture was progressively covered by new ectocranial deposits of bone that formed the posterior sagittal crest. This morphological difference might be related to the increased pressure exerted by the more developed posterior fibres of the temporalis muscle as *Thrinaxodon* grew.

Interestingly, the parietal-parietal suture in many modern mammals is one of the first sutures in the skull to obliterate/fuse (e.g., Herring, 1972; Wilson and Sánchez-Villagra, 2009; Sánchez-Villagra, 2010).

Interparietal suture. All specimens examined in this survey had a fused interparietal. Koyabu et al. (2012) showed that the interparietal is a single element in most therapsids; therefore it is unlikely that the interparietal was paired in the early ontogenetic stages of *Thrinaxodon*.

Unossified region: basioccipital-basisphenoid. The unossified zone between the basioccipital and basisphenoid is present in all ontogenetic stages of *Thrinaxodon*. The unossified zone appears to be a ubiquitous feature in therapsids because Olson (1938a,b, 1944) described it in anomodonts, gorgonopsians, therocephalians, and cynodonts. The unossified region of the skull was presumably filled with cartilage (Estes, 1961), and may have acted as a bone generating region in an animal that has continuous (indeterminate) growth.

Angulation of the zygomatic arch. Angulation of the zygomatic arch only occurs in two large adult specimens of *Thrinaxodon*, both which have a BSL larger than 90 mm. However, not all large specimens have this rare feature (Fig. 13), indicating individual variation in adult specimens of *Thrinaxodon*.

This is in contrast to the epicynodont *Galesaurus* (Fig. 1), where this feature is strongly correlated with skull size (Abdala, 2003; Abdala and Damiani, 2004). Angulation of the zygomatic arch was observed in most specimens of *Galesaurus* with a BSL of at least 90 mm, whereas it is mostly absent from smaller specimens (Abdala and Damiani, 2004; unpublished data). This strong size correlation suggests that this is an ontogenetic feature of *Galesaurus* (Abdala and Damiani, 2004). Although most large adult *Thrinaxodon* specimens lack this feature, it is interesting to note that it appears at ~90 mm BSL in both *Thrinaxodon* and *Galesaurus*.

In the adult specimens of the epicynodont *Progalesaurus* (BSL 93.5 mm; Fig. 1) and *Platycraniellus* (BSL 84 mm; Abdala, 2007), the angulation of the zygomatic arch is also present, although it is unknown if it was absent in smaller specimens.

In contrast to the epicynodonts, the angulation of the zygomatic arch occurs in all immature and adult chiniquodontid specimens (Abdala and Giannini, 2002; Fig. 1; Tables 4, 5). Therefore, in *Chiniquodon*, it is a ubiquitous feature independent of size or sex, which may indicate that the superficial masseter was more developed in the Chiniquodontia at an earlier stage, or that the superficialis was structurally more differentiated from the deep masseter.

The presence of the angulation of the zygomatic in these non-mammaliaform cynodonts suggests the presence of a superficial masseter muscle. Until the recent studies of Allin and Hopson (1992) and Abdala and Damiani (2004), it was presumed that epicynodonts possessed only an undivided masseter muscle (i.e., deep masseter) because they lack a distinctive suborbital process of the jugal. However, the comprehensive survey of non-mammaliaform cynodonts of Abdala and Damiani (2004) indicated that the angulation of the zygomatic arch in the Galesauridae more than likely indicates the origin of the M. superficialis masseter. Therefore, it is assumed that the masseter was divided near the base of the epicynodont clade (Abdala and Damiani, 2004), which includes *Thrinaxodon* (Fig. 1).

The superficial masseter inserted onto the dentary angle. A preliminary survey of the shape of the dentary angle indicates that *Thrinaxodon* has a weak, rounded dentary angle, whereas *Galesaurus* has a more prominent, sharp dentary angle. This difference, taken with the presence of angulation of the zygomatic in most large adult specimens of *Galesaurus*, lends support to the hypothesis that *Thrinaxodon* had a less-developed superficial masseter.

The superficial masseter had an anterodorsal orientation, whereas the deep masseter was oriented posterodorsally. If *Thrinaxodon* had a less-developed superficial masseter than in *Galesaurus*, then the pull of the mandible was mainly in the posterodorsal direction, as indicated by the deep masseter and the relatively stronger temporalis (Fig. 14).

External occipital crest and lambdoidal crest. The external occipital crest is present in most specimens with a BSL of 61 mm and greater; therefore it is an ontogenetic feature of *Thrinaxodon* (Table 6). Once formed, the low crest does not appear to become more developed with age, although more data from large adult specimens is needed.

van Heerden (1972) suggested that the temporal and nuchal muscles were more developed in older individuals, resulting in a posteriorly directed lambdoidal crest. However, the poor development of the external occipital crest in several specimens of *Thrinaxodon* suggests that the nuchal muscles were not strongly developed compared with the temporalis that originated from the well-developed sagittal crest. This in turn suggests that the posterior extension of the lambdoidal crest in larger specimens is more likely related to the development of the temporalis rather than the nuchal muscles.

Summary of the Qualitative Ontogenetic Features

After our comprehensive survey of *Thrinaxodon*, we have concluded that there are nine features of the skull that change during ontogeny (Table 6). Five of these features are present in the temporal region, whereas the remaining features are in the occiput, posterior palate, and snout (Table 6). In addition, there are ontogenetic changes in three dental features in the skull that were previously described by Abdala et al. (2013) (Table 6).

Taking into consideration all of these features, four distinct ontogenetic stages are recognized (Table 6): early juvenile (BSL $\leq$ 40 mm), late juvenile (BSL 42 mm), nonjuvenile or subadult (BSL 56–68 mm), and adult

(BSL $\geq$ 69 mm). We propose that the adult stage is defined by the appearance of the anterior sagittal crest, supported by the presence of a transverse nasal-frontal suture and a more complex upper postcanine morphology (Table 6). Growth continued even once the adult stage was reached, with the largest specimens attaining a BSL of 96 mm. The continued growth in adult specimens is supported by the presence of an unossified zone in the basicranium, and evidence of tooth replacement in large, presumably old individuals (e.g., BP/1/5905; BSL 87 mm) (Abdala et al., 2013).

Four of the ontogenetic features of *Thrinaxodon* involve changes in the suture morphology, including three features that can be easily observed on the dorsal and/or lateral surface of the skull and one feature (posterior parietal-parietal suture) that can only be determined through serial sectioning or micro-CT/CT scanning (Table 6). It is important to note that none of the cranial sutures in *Thrinaxodon* showed progressive fusion during ontogeny, even in specimens of large size. In the case of the posterior parietal-parietal suture, new bone was deposited on top of the suture to form a unified posterior sagittal crest.

Five of the cranial ontogenetic features listed in Table 6 are associated with changes in muscle function. This includes two features related to the development of the sagittal crest and the associated temporalis musculature. The earlier development of the posterior sagittal crest and the ectocranial apposition of bone suggest that the posterior fibres of the temporalis muscle became much more developed with increasing age. Another ontogenetic feature related to the temporalis musculature is the change in the posterior projection of the postorbital bone. The lengthening of the dorsal and ventral processes might have assisted with the stabilization of the postorbital bar and reduced the muscle-related stresses in the anterior temporal region. The fourth ontogenetic feature is the appearance of a low external occipital crest in most mature individuals, which likely is associated with the development of the nuchal muscles. However, this crest is absent from a few adult specimens and the crest does not appear to develop greatly with age, which suggests that the nuchal muscles were not well-developed. And lastly, the loss of the interpterygoid vacuities might be partially related to the development of the pterygoideus musculature (Estes, 1961), although this region also might have been transformed because it was a growth zone (see Martinelli, 2009).

Despite a large number of *Thrinaxodon* specimens included in this study, a gap remains between 42 mm and 56 mm of BSL (Fig. 4), during which at least three important cranial changes occurred (Table 6). At 56 mm BSL, the intermediate-sized specimen TM 80A is an important bridge between the juvenile and adult specimens. Specimen TM 80A had gained some of the features characteristic of adults: the nasal-frontal suture is transverse, the paired interpterygoid vacuities are absent, the frontal-parietal suture is interdigitated, and the posterior projection of the postorbital is C-shaped (Table 6). In this specimen, however, the anterior sagittal crest has not yet developed, the supraoccipital projects far posteriorly, and the external occipital crest is absent, all features that it shares with immature specimens. Our allometric study of the large sample of *Thrinaxodon* agrees with this as TM 80A plots between the two groups of specimens considered to be juveniles and adults (Fig. 4).

Summary of the Cranial Function of *Thrinaxodon*

The length of the temporal region of *Thrinaxodon* shows strong positive allometry (Table 3), indicating this region grew much faster than the rest of the skull and could therefore accommodate a large, well-developed temporalis muscle. Greater development of the posterior part of the temporal region of *Thrinaxodon* is indicated by: (1) earlier development of the posterior sagittal crest at a younger age compared to the anterior crest, suggesting that the posterior fibres of the temporalis developed earlier in ontogeny; (2) deposition of new bone onto the dorsal surface of the posterior parietals to form a unified posterior sagittal crest, which is in contrast to the patent parietal-parietal suture of the anterior sagittal crest that spanned the entire depth of the skull roof; and (3) the lambdoidal crest became more posteriorly directed during ontogeny suggesting the posterior temporalis became much larger with age. Therefore, it is clear that during growth of *Thrinaxodon*, the posterior sagittal crest was emphasized, indicating a greater development of the temporalis muscle in this region.

On the other hand, it appears that the masseter muscles were not as well-developed as the temporalis in *Thrinaxodon*. The lateral flaring of the zygomatic arches, which defines the area for the developing deep masseter, only increased isometrically or negatively with age (Table 3). The height of the zygomatic arch is isometric, and so the masseter muscles (especially the deep portion) would have been proportionally less developed in comparison with the three eucynodonts (Table 5). The rare occurrence of the angulation of the zygomatic arch in *Thrinaxodon* also corroborates the limited development of the superficial masseter in this taxon.

CONCLUSIONS

A combination of quantitative and qualitative analyses has enabled a comprehensive survey of ontogenetic changes and intraspecific variability in *Thrinaxodon liorhinus*. With 60 specimens analyzed, this is the most thorough allometric study of any non-mammaliaform cynodont taxon (Table 4). The bivariate analysis indicated that the temporal region, snout, and palate showed positive allometry during the growth of *Thrinaxodon*. The strong positive allometry of the temporal region indicated that this area grew much faster than the rest of the skull and suggests that the temporalis muscle was well-developed. This trend was also supported by several qualitative ontogenetic changes that were observed in the intertemporal region of *Thrinaxodon*.

Our qualitative survey of 68 specimens found nine cranial characters that change during the ontogeny of *Thrinaxodon*. Taking into account these qualitative characters, our sample was divided into four discrete ontogenetic stages: early juvenile, late juvenile, subadult, and adult. It appears that even when the adult stage was reached at 69 mm of BSL, *Thrinaxodon* had continuous (indeterminate) growth. It is anticipated that when the size gap between late juvenile (BSL 42 mm) and subadult specimens (BSL 56 mm) is narrowed with further

collection of specimens, the timing of several important changes that occurred in the skull (Table 6) will be resolved.

Future studies include investigations of cranial ontogeny of other basal cynodonts, such as *Galesaurus* and *Procynosuchus*, to understand the functional significance of the ontogenetic changes of *Thrinaxodon* within a broader evolutionary context.

ACKNOWLEDGEMENTS

The authors thank C. Churms (DebTech, DeBeers, ZA), P. Keanly (X-Sight, ZA), and P. Tafforeau (ESRF, FR) for micro-CT scanning specimens of *Thrinaxodon*. The specimens BP/1/7199 and BP/1/5905 were scanned during experiment EC-847. The curators and collection managers of the following institutions are acknowledged for allowing access to their specimens: AMMM, BP, BSP, FMNH, MCZ, NHMUK, NMQR, RC, SAM, TM, UCMP, UMZC, and USNM. For help providing photos from specimens the authors thank R. Asher, G. Bever, E. Butler, H. Fourie, L. Gaetano, J. Liu, M. Lowe, T. Martin, G. Oleschinski, and O. Rauhut. They also thank C. Dube, S. Jirah and T. Nemavhundi (ESI, Witswatersrand) for further preparation of some specimens. Additional thanks are given to the two anonymous reviewers, and S. Herring and E. Allin for their helpful comments.

LITERATURE CITED

Abdala F. 2003. Galesaurid cynodonts from the Early Triassic of South Africa: another example of conflicting distribution of characters in non-mammalian cynodonts. South African J Sci 99: 95–96.

Abdala F. 2007. Redescription of *Platycraniellus elegans* (Therapsida, Cynodontia) from the lower Triassic of South Africa, and the cladistic relationships of eutheriodonts. Palaeontology 50: 591–618.

Abdala F, Allinson M. 2005. The taxonomic status of *Parathrinaxodon proops* (Therapsida: Cynodontia), with comments on the morphology of the palate in basal cynodonts. Palaeontol Africana 41:45–52.

Abdala F, Damiani R. 2004. Early development of the mammalian superficial masseter muscle in cynodonts. Palaeontol Africana 40: 23–29.

Abdala F, Giannini NP. 2000. Gomphodont cynodonts of the Chanares Formation: the analysis of an ontogenetic sequence. J Vertebr Paleontol 20:501–506.

Abdala F, Giannini NP. 2002. Chiniquodontid cynodonts: systematic and morphometric considerations. Palaeontology 45:1151–1170.

Abdala F, Flores DA, Giannini NP. 2001. Postweaning ontogeny of the skull of *Didelphis albiventris*. J Mammal 82:190–200.

Abdala F, Jasinoski SC, Fernandez V. 2013. Ontogeny of the Early Triassic cynodont *Thrinaxodon liorhinus* (Therapsida): dental morphology and replacement. J Vertebr Paleontol 33:1408–1431.

Alexander RM. 1985. Body support, scaling and allometry. In: Hildebrand M, Wake DB, editors. Functional vertebrate morphology. Cambridge: The Belknap Press of Harvard University Press. p. 27–37.

Allin EF, Hopson JA. 1992. Evolution of the auditory system in Synapsida ("Mammal-like reptiles" and primitive mammals) as seen in the fossil record. In: Webster DB, Fay RR, Popper AN, editors. The evolutionary biology of hearing. New York: Springer-Verlag. p 587–614.

Anderson JS, Reisz RR. 2004. *Pyozia mesenensis*, a new, small varanopid (Synapsida, Eupelycosauria) from Russia: "pelycosaur" diversity in the Middle Permian. J Vertebr Paleontol 24:173–179.

Barghusen HR. 1968. The lower jaw of cynodonts (Reptilia, Therapsida) and the evolutionary origin of mammal-like adductor jaw musculature. Postilla 116:1–49.

Barghusen HR. 1972. The origin of the mammalian jaw apparatus. In: Schumacher G, editor. Morphology of the maxillo-mandibular apparatus. Leipzig: VEB Georg Thieme. p 26–32.

Barghusen HR. 1986. On the evolutionary origin of the therian tensor veli palatini and tensor tympani muscles. In: Hotton N, MacLean PD, Roth JJ, Roth EC, editors. The ecology and biology of mammal-like reptiles. Washington: Smithsonian Institutional Press. p 253–262.

Botha J, Abdala F, Smith RMH. 2007. The oldest cynodont: new clues on the origin and early diversification of the Cynodontia. Zool J Linn Soc 149:477–492.

Botha J, Chinsamy A. 2005. Growth patterns of *Thrinaxodon liorhinus*, a non-mammalian cynodont from the lower Triassic of South Africa. Palaeontology 48:385–394.

Botha J, Smith R. 2006. Rapid vertebrate recuperation in the Karoo Basin of South Africa following the End-Permian extinction. J African Earth Sci 45:502–514.

Bradu D, Grine FE. 1979. Multivariate analysis of diademodontine crania from South Africa and Zambia. South Af J Sci 75:441–448.

Brink AS. 1955. Note on a very tiny specimen of *Thrinaxodon liorhinus*. Palaeontol Africana 3:73–76.

Broom R. 1938. On the structure of the skull of the cynodont, *Thrinaxodon liorhinus*, Seeley. Ann Transvaal Museum 19:263–269.

Carroll RL. 1988. Vertebrate paleontology and evolution. New York: W.H. Freeman and Company.

Cohen MM, Jr. 2005. Perspectives on craniosynostosis. Am J Med Genet 136A:313–326.

Crompton AW. 1955. A revision of the Scaloposauridae with special reference to kinetism in this family. Navors Nas Mus, Bloemfontein 1:149–183.

Elbroch, M. 2006. Animal skulls. A guide to North American species. Mechanicsburg: Stackpole Books.

Emerson S, Bramble D. 1993. Scaling, allometry, and skull design. In: Hanken J, Hall BK, editors. The skull, Vol. 3. Chicago: University of Chicago Press. p 384–421.

Estes R. 1961. Cranial anatomy of the cynodont reptile *Thrinaxodon liorhinus*. Bull the Mus Comp Zool 125:165–180.

Evans HE. 1993. Miller's anatomy of the dog. 3rd ed. Philadelphia: W.B. Saunders Company.

Flores DA, Giannini N, Abdala F. 2006. Comparative postnatal ontogeny of the skull in the australidelphian metatherian *Dasyurus albopunctatus* (Marsupialia: Dasyuromorpha: Dasyuridae). J Morphol 267:426–440.

Fourie S. 1974. The cranial morphology of *Thrinaxodon liorhinus* Seeley. Annal South Af Mus 65:337–400.

Garcia-Perea R. 1996. Patterns of postnatal development in skulls of lynxes, genus *Lynx* (Mammalia: Carnivora). J Morphol 229: 241–254.

Giannini NP, Abdala F, Flores DA. 2004. Comparative postnatal ontogeny of the skull of *Dromiciops gliroides* (Marsupialia: Microbiotheriidae). Am Mus Novitates 3460:1–17.

Grine FE, Hahn BD. 1978. Allometric growth in the Diademodontinae (Reptilia; Therapsida): a preliminary report. Palaeontol Africana 21:161–166.

Grine FE, Hahn BD, Gow CE. 1978. Aspects of relative growth and variability in *Diademodon* (Reptilia; Therapsida). South Af J Sci 74:50–58.

Hammer Ø, Harper DAT. 2006. Paleontological data analysis. MA, USA: Blackwell Publishing.

Hammer Ø, Harper DAT, Ryan PD. 2001. PAST: Paleontological statistics software package for education and data analysis. Palaeontol Electron 4:9. Available at: http://palaeo-electronica.org/2001_1/past/issue1_01.htm.

Herrel A, O'Reilly JC, Richmond AM. 2002. Evolution of bite performance in turtles. J Evol Biol 15:1083–1094.

Herring SW. 1972. Sutures—a tool in functional cranial analysis. Acta Anat 83:222–247.

Holbrook LT. 2002. The unusual development of the sagittal crest in the Brazilian tapir (*Tapirus terrestris*). J Zool 256:215–219.

Holz M, Schultz CL. 1998. Taphonomy of the south Brazilian Triassic herpetofauna: fossilization mode and implications for morphological studies. Lethaia 31:335–345.

Hopson JA. 1991. Systematics of the nonmammalian Synapsida and implications for patterns of evolution in synapsids. In: Schultze H-P, Trueb L, editors. Origins of the higher groups of tetrapods. Ithaca: Comstock Publishing Associates. p 635–693.

Hopson JA, Barghusen HR. 1986. An analysis of therapsid relationships. In: Hotton N, MacLean PD, Roth JJ, Roth EC, editors. The ecology and biology of mammal-like reptiles. Washington: Smithsonian Institutional Press. p 83–106.

Huttenlocker AK, Abdala F. Revision of the first therocephalian, *Theriognathus* Owen (Therapsida: Whaitsiidae), and implications for cranial ontogeny and allometry in nonmammaliaform eutheriodonts. J Paleontol (in press).

Kemp TS. 2005. The origin and evolution of mammals. Oxford: Oxford University Press.

Kermack KA. 1972. The origin of mammals and the evolution of the temporomandibular joint. Proc Roy Soc Med 65:389–392.

Koyabu D, Maier W, Sánchez-Villagra MR. 2012. Paleontological and developmental evidence resolve the homology and dual embryonic origin of a mammalian skull bone, the interparietal. Proc Natl Acad Sci U S A 109:14075–14080.

Langston W, Reisz RR. 1981. *Aerosaurus wellesi*, new species, a varanopseid mammal-like reptile (Synapsida: Pelycosauria) from the Lower Permian of New Mexico. J Vertebr Paleontol 1:73–96.

Liu J, Soares MB, Reichel M. 2008. *Massetognathus* (Cynodontia, Traversodontidae) from the Santa Maria Formation of Brazil. Rev Bras de Paleontol 11:27–36.

Markey MJ. and Marshall CR. 2007. Linking form and function of the fibrous joints in the skull: a new quantification scheme for cranial sutures using the extant fish *Polypterus endlicherii*. J Morphol 268:82–102.

Martinelli AG. 2009. Interpterigoid vacuities in the primary palate of cynodonts (Therapsida): heterochrony and evolutionary significance. Actas del 4to. Encuentro Internacional del International Center of Earth Sciences (E-ICES-4), Malargüe, Mendoza, p 1–11.

Olson EC. 1938a. The occipital, otic, basicranial and pterygoid regions of the Gorgonopsia. J Morphol 62:141–175.

Olson EC. 1938b. Notes on the brain case of a therocephalian. J Morphol 63:75–86.

Olson EC. 1944. Origin of mammals based upon cranial morphology of the therapsid suborders. Geol Soc Am Special Paper 55:136.

Owen R. 1887. On the skull and dentition of a Triassic saurian (*Galesaurus planiceps*, Ow.) Quart J Geol Soc 43:1–6.

Parrington FR. 1935. A note on the parasphenoid of the cynodont *Thrinaxodon liorhinus* Seeley. Ann Mag Nat History 16:399–401.

Parrington FR. 1936. On the tooth-replacement in Theriodont reptiles. Phil Trans R Soc Lond. Series B 226:121–142.

Parrington FR. 1946. On the cranial anatomy of cynodonts. Proc Zool Soc Lond 116:181–197.

Rafferty KL, Herring SW, Marshall CD. 2003. Biomechanics of the rostrum and the role of facial sutures. J Morphol 257:33–44.

Rowe T, Carlson W, Bottorff W. 1993. *Thrinaxodon*: digital atlas of the skull. CD-ROM (First edition, for MS-DOS platform), University of Texas Press, 623 megabytes.

Sánchez-Villagra MR. 2010. Suture closure as a paradigm to study late growth in recent and fossil mammals: a case study with giant deer and dwarf deer skulls. J Vertebr Paleontol 30:1–4.

Seeley HG. 1894. Researches on the structure, organization, and classification of the fossil Reptilia. Part IX. Section 1. On the Theriosuchia. Phil Trans R Soc Lond Ser B 185:987–1018.

Sidor CA, Smith RMH. 2004. A new galesaurid (Therapsida: Cynodontia) from the Lower Triassic of South Africa. Palaeontology 47:535–556.

Thomason JJ, Russell AP. 1986. Mechanical factors in the evolution of the mammalian secondary palate: A theoretical analysis. J Morphol 189:199–213.

Tonge CH, Luke DA. 1985. Dental anatomy: the palate. MGDS RCS examination. p. 461–467.

van Heerden J. 1972. Interspecific variation and growth changes in the cynodont reptile *Thrinaxodon liorhinus*. Novors van die Nas Mus 2:307–347.

Wang Q, Straight DS, Dechow PC. 2006. Fusion patterns of craniofacial sutures in rhesus monkey skulls of known age and sex from Cayo Santiago. Am J Phys Anthropol 131:469–485.

Washburn SL. 1947. The relation of the temporal muscle to the form of the skull. Anat Rec 99:239–248.

Wilson LAB, Sánchez-Villagra MR. 2009. Heterochrony and patterns of cranial suture closure in hysticognath rodents. J Anat 214:339–354.

Wolpoff ML. 1974. Sagittal cresting in the South African australopithecines. Am J Phys Anthropol 40:397–408.